Cell Reports

Early Seizure Activity Accelerates Depletion of Hippocampal Neural Stem Cells and Impairs Spatial Discrimination in an Alzheimer's Disease Model

Graphical Abstract

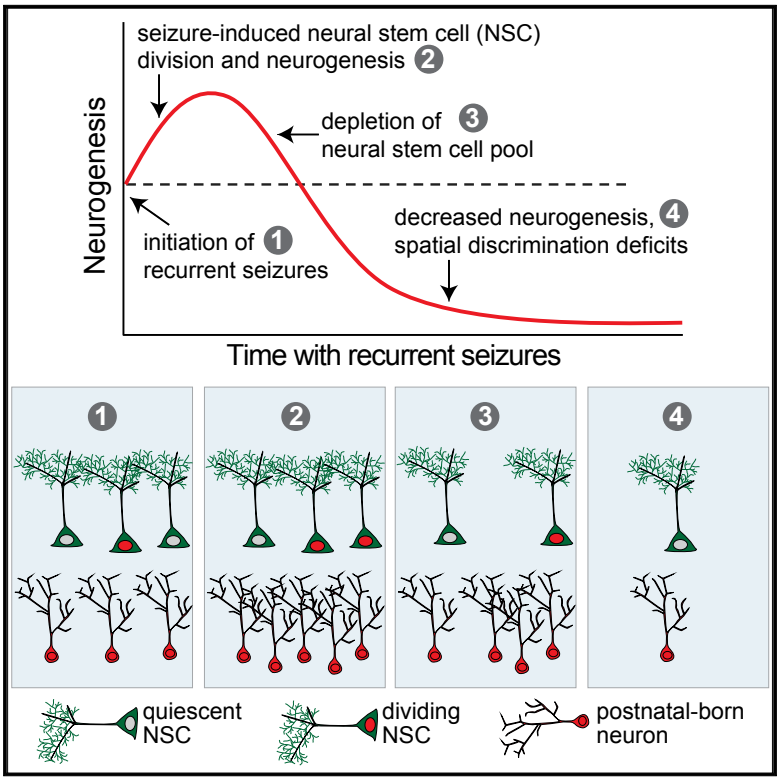

Highlights

- Seizure-induced NSC proliferation in AD mice accelerates the depletion of the finite NSC pool
- Hippocampal neurogenesis is increased early, but decreased later, in disease
- Reduced neurogenesis coincides with deficits in spatial discrimination in AD mice
- Antiseizure drug normalizes neurogenesis and improves spatial discrimination in AD mice

Authors

Chia-Hsuan Fu, Daniel Maxim Iascone, Iraklis Petrof, ..., Helen E. Scharfman, Grigori Enikolopov, Jeannie Chin

Correspondence

jeannie.chin@bcm.edu

In Brief

The mechanisms that alter hippocampal neurogenesis in AD patients and mice are unclear. Fu et al. show that in a transgenic mouse model, spontaneous seizures stimulate neural stem cell (NSC) proliferation and accelerate depletion of a finite NSC pool. This process leads to neurogenesis that is increased early but decreased later in disease, coinciding with spatial discrimination deficits.

Fu et al., 2019, Cell Reports 27, 3741–3751
June 25, 2019
https://doi.org/10.1016/j.celrep.2019.05.101

CellPress

Cell Reports
Report

Early Seizure Activity Accelerates Depletion of Hippocampal Neural Stem Cells and Impairs Spatial Discrimination in an Alzheimer's Disease Model

Chia-Hsuan Fu,[1,2,5] Daniel Maxim Iascone,[2,5,6] Iraklis Petrof,[1,2,7] Anupam Hazra,[2,8] Xiaohong Zhang,[2,9] Mark S. Pyfer,[2,10] Umberto Tosi,[2,11] Brian F. Corbett,[2,12] Jingli Cai,[2] Jason Lee,[1] Jin Park,[1] Lorraine Iacovitti,[2] Helen E. Scharfman,[3] Grigori Enikolopov,[4] and Jeannie Chin[1,2,13,*]

[1]Memory & Brain Research Center, Department of Neuroscience, Baylor College of Medicine, Houston, TX 77030, USA
[2]Department of Neuroscience and Farber Institute for Neurosciences, Thomas Jefferson University, Philadelphia, PA 19107, USA
[3]Departments of Psychiatry, Neuroscience, and Physiology and the Neuroscience Institute, New York University Langone Medical Center, New York, NY 10016, USA
[4]Center for Developmental Genetics and Department of Anesthesiology, Renaissance School of Medicine, Stony Brook University, Stony Brook, NY 11794, USA
[5]These authors contributed equally
[6]Present address: Columbia University, New York, NY 10027, USA
[7]Present address: Children's Hospital of Philadelphia, Philadelphia, PA 19104, USA
[8]Present address: Institute for Stem Cell Science and Regenerative Medicine, Bengaluru, Karnataka 560065, India
[9]Present address: Children's Hospital of Philadelphia, Philadelphia, PA 19104, USA
[10]Present address: University of Pennsylvania, Philadelphia, PA 19104, USA
[11]Present address: Joan & Sanford I. Weill Medical College, Cornell University, New York, NY 10065, USA
[12]Present address: Children's Hospital of Philadelphia, Philadelphia, PA 19104, USA
[13]Lead Contact
*Correspondence: jeannie.chin@bcm.edu
https://doi.org/10.1016/j.celrep.2019.05.101

SUMMARY

Adult hippocampal neurogenesis has been reported to be decreased, increased, or not changed in Alzheimer's disease (AD) patients and related transgenic mouse models. These disparate findings may relate to differences in disease stage, or the presence of seizures, which are associated with AD and can stimulate neurogenesis. In this study, we investigate a transgenic mouse model of AD that exhibits seizures similarly to AD patients and find that neurogenesis is increased in early stages of disease, as spontaneous seizures became evident, but is decreased below control levels as seizures recur. Treatment with the antiseizure drug levetiracetam restores neurogenesis and improves performance in a neurogenesis-associated spatial discrimination task. Our results suggest that seizures stimulate, and later accelerate the depletion of, the hippocampal neural stem cell pool. These results have implications for AD as well as any disorder accompanied by recurrent seizures, such as epilepsy.

INTRODUCTION

Alzheimer's disease (AD) is characterized by prominent impairments in memory (Holtzman et al., 2011; Weintraub et al., 2012). Many studies have therefore focused on the hippocampus, which is critical for memory formation and is exquisitely vulnerable to dysfunction (Fjell et al., 2014; Leal and Yassa, 2013; Morrison and Hof, 2002). The hippocampus is also important for mood regulation, which is also affected in AD (Kheirbek et al., 2013; Sala et al., 2004). The amyloid precursor protein (APP) and the amyloid beta (Aβ) peptides cleaved from it play central roles in AD (Bertram et al., 2010; Mucke and Selkoe, 2012); however, the precise mechanisms by which Aβ impairs neuronal function are unclear. One mechanism may be through disruption of adult hippocampal neurogenesis. Aβ affects neural stem cell (NSC) dynamics *in vitro* (Haughey et al., 2002; Sotthibundhu et al., 2009), and transgenic mice that produce high levels of Aβ exhibit alterations in adult hippocampal neurogenesis (Mu and Gage, 2011; Rodríguez and Verkhratsky, 2011). Importantly, adult neurogenesis is involved in both memory and mood, and it is altered in AD (Aimone et al., 2014; Anacker and Hen, 2017; Christian et al., 2014; Jin et al., 2004b; Miller and Hen, 2015; Moreno-Jiménez et al., 2019).

Neurogenesis in the hippocampal dentate gyrus (DG) continues beyond development, although to diminished levels relative to the developing brain (Bergmann et al., 2015; Knoth et al., 2010). A number of studies have demonstrated evidence of post-natal neurogenesis in adult humans (Boldrini et al., 2018; Eriksson et al., 1998; Ernst et al., 2014; Kempermann et al., 2018; Moreno-Jiménez et al., 2019; Spalding et al., 2013; but see Sorrells et al., 2018). Although it is difficult to examine its function in humans, postnatal neurogenesis has been well studied in rodents, which has advanced our knowledge of the cognitive and psychiatric domains modulated by adult-born neurons. Adult-born granule cells in the DG are important for mood regulation

as well as spatial discrimination, the ability to distinguish between similar but different contexts (Aimone et al., 2011; Danielson et al., 2016; Nakashiba et al., 2012). Spatial discrimination is impaired in AD patients and related mouse models (Ally et al., 2013; Richetin et al., 2015; Salmon, 2012; Wesnes et al., 2014), but the underlying mechanisms remain unclear, perhaps due in part to conflicting reports about how adult neurogenesis is altered in AD. Studies have found increased, decreased, or no changes in hippocampal neurogenesis in AD patients (Boekhoorn et al., 2006; Briley et al., 2016; Jin et al., 2004b; Mu and Gage, 2011; Rodríguez and Verkhratsky, 2011). A recent study demonstrated not only the robust presence of adult neurogenesis in older humans, but also consistent decreases in neurogenesis in AD patients (Moreno-Jiménez et al., 2019). Varied alterations in neurogenesis have also been described in transgenic mice that express high levels of Aβ (Chevallier et al., 2005; Donovan et al., 2006; Hamilton et al., 2010; Jin et al., 2004a; Krezymon et al., 2013; López-Toledano and Shelanski, 2007; Rodríguez et al., 2008; Taniuchi et al., 2007; Unger et al., 2016; Verret et al., 2007; Zhang et al., 2007). These disparate results may reflect different stages of disease progression, or the degree to which patients exhibit other symptoms such as seizures, which can directly alter neurogenesis (Mu and Gage, 2011).

Indeed, in experimental models of seizures, hippocampal NSC proliferation increases rapidly after seizure onset, consistent with evidence that increases in neuronal activity increase proliferation (Gray and Sundstrom, 1998; Nakagawa et al., 2000; Parent et al., 2006; Scharfman and Gray, 2007). After severe seizures such as status epilepticus (SE), there is also a rapid increase in proliferation of both NSCs and glia within the first hours to days, and then an increase in newborn neurons starting about 4 days after SE. However, in conditions in which seizures are recurrent, the numbers of newborn neurons are typically reduced (Hattiangady et al., 2004; Ledergerber et al., 2006).

AD patients also exhibit epileptiform activity and spontaneous seizures that begin early in disease progression, often in the fifth or sixth decade of life. Some of these individuals carry familial mutations linked to AD (Hauser et al., 1986; Lozsadi and Larner, 2006; Scarmeas et al., 2009), but subclinical epileptiform activity has also been documented in patients with no known familial mutations (Lam et al., 2017; Vossel et al., 2013, 2016). Transgenic mice that express mutant human APP also have recurrent seizures (Chin and Scharfman, 2013; Kam et al., 2016; Minkeviciene et al., 2009; Palop et al., 2007). Therefore, the recurrent seizures in AD and epilepsy may initiate an acute increase, but subsequent reduction, in neurogenesis in the long term. One mechanism that could explain the early increase and later reduction in neurogenesis is that some populations of NSCs have a finite capability to produce neuronal cells, suggesting that excessive stimulation of NSC division may exhaust the NSC pool (Encinas et al., 2011b; Pilz et al., 2018). Recurrent seizures can lead to an accelerated depletion of the NSC pool (Sierra et al., 2015). However, how the NSC pool is regulated in AD models throughout disease progression, and whether seizure activity plays any role, is not clear. In this study, we tested the hypothesis that the hippocampal NSC pool is prematurely exhausted in a transgenic APP mouse model of AD that exhibits spontaneous recurrent seizures (line J20, Mucke et al., 2000).

RESULTS

The Rate of Adult Hippocampal Neurogenesis in APP Mice Increases after Seizure Activity Starts and then Decreases with Age

Pharmacologically induced seizures acutely increase neurogenesis in the DG (Gray and Sundstrom, 1998; Nakagawa et al., 2000; Parent et al., 2006). However, in chronic stages of epilepsy, neurogenesis is reduced below control levels (Hattiangady et al., 2004), which has been hypothesized to result from the seizure-induced depletion of the NSC pool (Sierra et al., 2015; see also Figure 1A). Because APP mice exhibit spontaneous seizures, we assessed whether neurogenesis follows a similarly biphasic dynamic during disease progression. In this line of APP mice, epileptic spikes are evident by 1 month of age, and seizures are robust by 2 months of age (Figures 1B–1D). To test if neurogenesis is altered as seizures develop in APP mice, we performed immunophenotyping, which identifies cell types based on cell morphology and expression of cell-specific markers (as in Encinas and Enikolopov, 2008). Using doublecortin (DCX) to assess immature neurons (Figure 1E), we found that relative to nontransgenic (NTG) controls, APP mice exhibited similar numbers of immature neurons at 1 month of age, but increased numbers by 2 months of age (Figures 1F and 1G). The number of immature neurons was reduced below NTG levels at 3, 7, and 14 months of age (Figure 1G), as was the number of neuroblasts (Figure S1A). DCX-expressing immature neurons also expressed PSA-NCAM and β3-tubulin, confirming their identity (Figure S2). We also tested whether other APP transgenic lines that exhibit seizures exhibit similar alterations in neurogenesis. We found that the number of immature neurons in transgenic PS1-APP mice was increased at younger ages and decreased at older ages, relative to NTG littermates (Figures S3A and S3B). In addition, aged Tg2576 mice also had fewer immature neurons relative to NTG littermates (Figure S3C). These results are similar to our findings in J20 APP mice and support the hypothesis that seizures alter neurogenesis in APP mice.

Studies of seizure-induced neurogenesis in pharmacological models of epilepsy showed that neurons born postnatally into an epileptic hippocampus can exhibit altered morphology and ectopic migration (Jessberger et al., 2007; Parent, 2007; Scharfman et al., 2000). We found that DCX-expressing immature neurons in a pilocarpine mouse model of epilepsy exhibited altered morphology with disorganized neurites as well as ectopic migration into the hilus (Figure S4A), as previously described (Myers et al., 2013; Scharfman et al., 2000). We did not find obvious morphological differences in DCX-expressing immature neurons in APP mice, although we did find a small increase in the number of ectopic granule neurons in the hilus (Figures S4A–S4C). These results may reflect differences in seizure severity and frequency, which is greater in pilocarpine-induced epilepsy than what occurs spontaneously in APP mice.

APP Mice Exhibit Increased NSC Division Followed by Accelerated NSC Pool Depletion

To assess whether the initial increase and subsequent decrease in neurogenesis in APP mice corresponds to changes in NSC

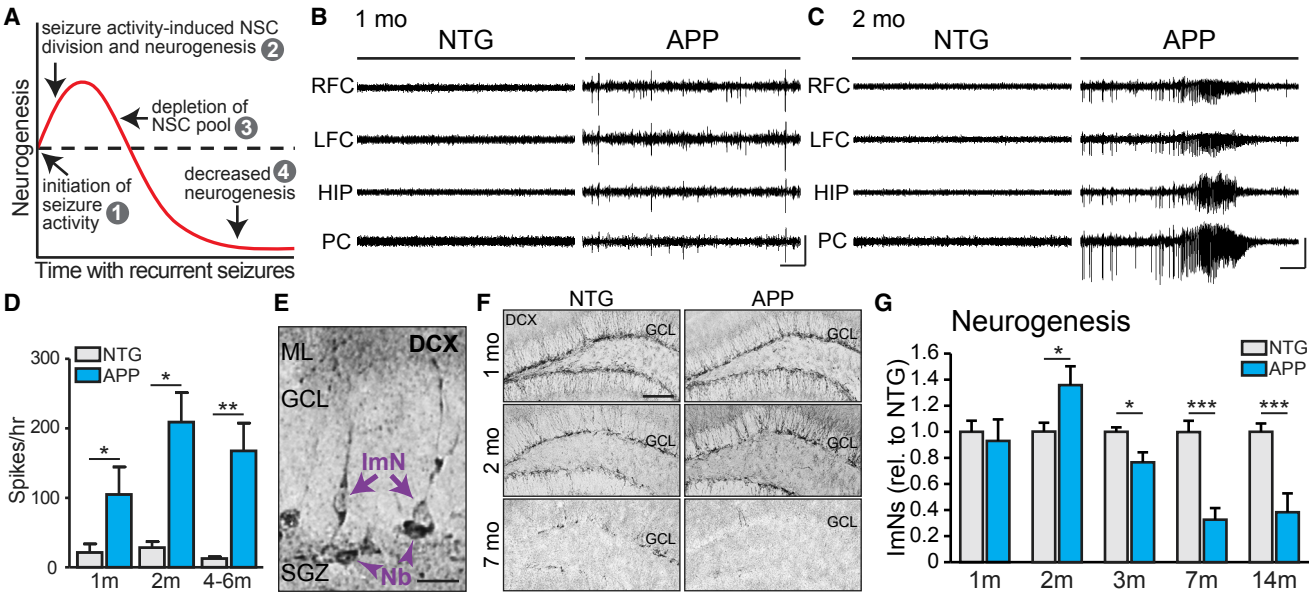

Figure 1. The Rate of Adult Hippocampal Neurogenesis in APP Mice Increases after Seizure Activity Starts and Then Decreases with Age

(A) Model illustrating how seizure activity may induce changes in neurogenesis.

(B and C) Representative electroencephalogram (EEG) traces from NTG and APP mice at 1 and 2 months of age, with epileptiform spikes at 1 month of age (B) and a seizure at 2 months of age (C) in APP mice. Electrodes were in left and right frontal cortices (LFC and RFC), hippocampus (HIP), and parietal cortex (PC). Scale bars, 1 mV, 10 s.

(D) The number of epileptic spikes per hour in NTG or APP mice at 1, 2, and 4–6 months of age (n = 3–5 mice per genotype and age).

(E) Immunophenotyping of immature neurons (ImN) and neuroblasts (Nb) by examining morphology of cells that express doublecortin (DCX). Scale bar, 20μm.

(F) DCX staining in NTG and APP mice at 1, 2, and 7 months of age. Scale bar, 100 μm.

(G) DCX expression at 1 month of age (n = 9–12 mice per genotype) and number of DCX+ ImNs at 2 (n = 6 mice per genotype), 3 (n = 8 mice per genotype), 7 (n = 9–10 mice per genotype), and 14 (n = 11–12 mice per genotype) months of age, normalized to NTG at each time point.

*p < 0.05; **p < 0.01; ***p < 0.001; two-tailed unpaired Student's t test comparing means between NTG and APP mice at each age. Values indicate mean ± SEM. See also Figures S1–S4 and Tables S1 and S2.

numbers, we quantified NSCs at different ages. In wild-type mice, the number of NSCs declines with aging (Encinas et al., 2011b), but whether this process is the same in APP mice was not clear. We immunophenotyped nestin-positive cells with radial glia-like morphology (Figure 2A; as in Encinas and Enikolopov, 2008) and found that APP and NTG mice had similar numbers of NSCs at 1 month of age, and both genotypes exhibited age-dependent decreases in NSC numbers (Figures 2B and 2C). However, compared to NTG mice, APP mice exhibited an accelerated loss of NSCs, such that by 2 months of age and onward, there were fewer total NSCs in APP mice than in NTG controls (Figures 2B and 2C). NSCs were similarly reduced in PS1-APP and Tg2576 mice (Figures S3D–S3F).

To test if the accelerated loss of NSCs in APP mice could be due to excessive cell division, leading to a depletion of the NSC pool, we administered the thymidine analog BrdU as a marker of cell division. We assessed the number of BrdU+ NSCs in APP and NTG mice at different ages (Figures 2D–2F). We found an initial increase in the numbers of dividing NSCs in APP mice at 1 month of age (Figures 2E and 2F), no change at 2 months of age, and a reduction by 3 months of age (Figures 2E and 2F; see Figures S1B and S1C for ANPs and dividing ANPs). We noted that at 2 months of age, APP mice had similar levels of dividing NSCs, but fewer total NSCs than NTG mice. Therefore, the rate of division relative to NTG mice was proportionally increased at that time point (Figure 2F inset; see Figure S5 for rates of division at other time points). We obtained similar results using Ki67 as an independent marker of cell division (Figures 2G–2I).

APP Mice Have a Higher Fraction of NSCs Engaged in Consecutive Divisions Early in Life than NTG Mice Do

When NSCs divide, they can divide consecutively 3 or 4 times to produce neuronal precursors before exiting the stem cell pool (Encinas et al., 2011b, 2006). If this process is altered in APP mice such that NSCs do not divide consecutively, the accelerated loss of NSCs in APP mice might be due to fundamental differences in the process of neurogenesis, not due to accelerated usage. To test this possibility, we administered BrdU and EdU 22 h apart and collected brains 2 h after EdU injection. NSCs dividing on day 1 of the injection with BrdU, but not on day 2 with EdU, should only incorporate BrdU labeling. NSCs dividing only on day 2 should only incorporate EdU labeling. NSCs that divided on day 1 and then immediately reentered the cell cycle to divide again on day 2 ("consecutively dividing") should incorporate both BrdU and EdU (Figure 3A; as in Encinas et al., 2011b). Both APP and NTG mice exhibited age-dependent decreases in numbers of consecutively dividing

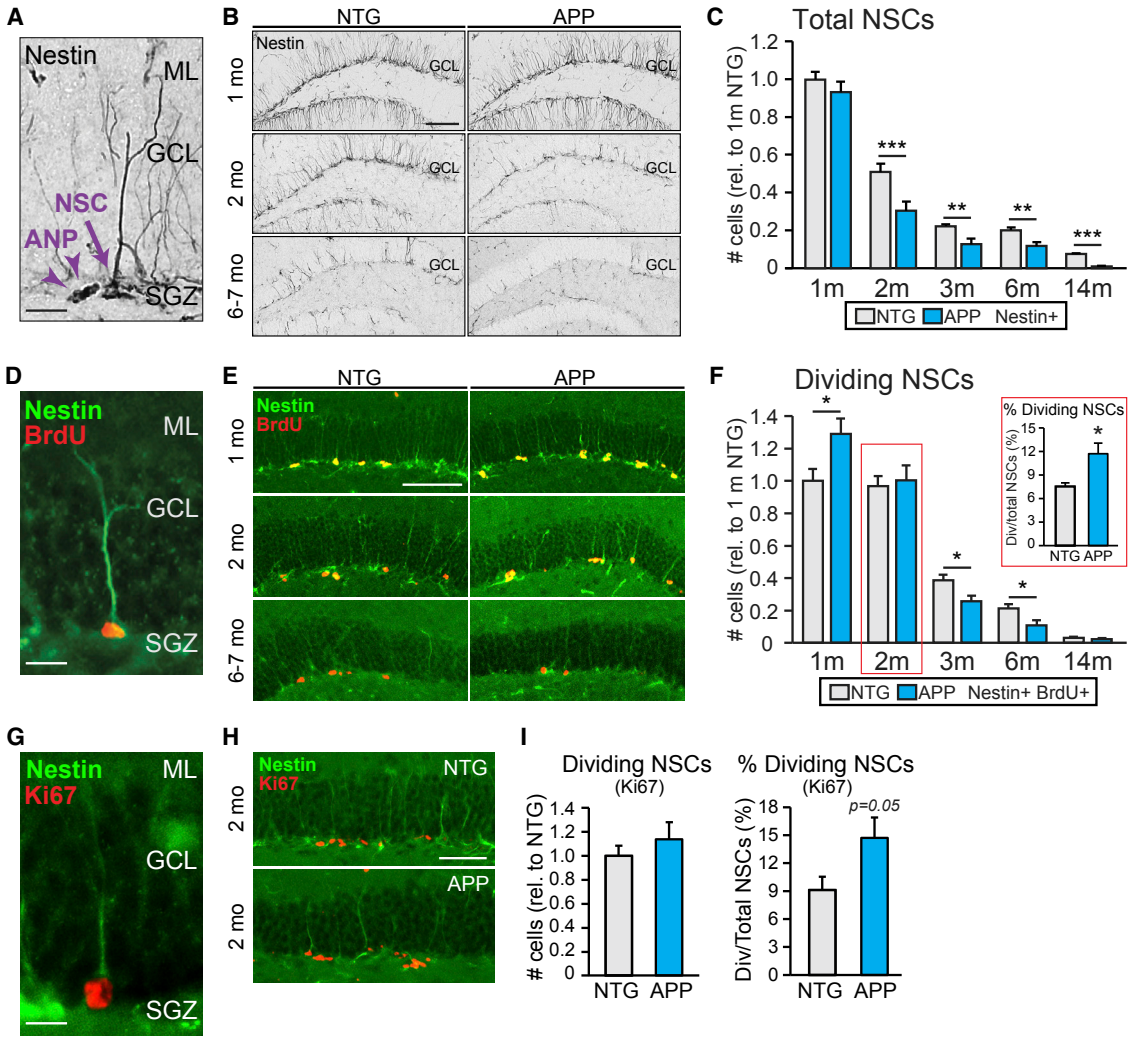

Figure 2. APP Mice Exhibit Increased NSC Division Followed by Accelerated NSC Pool Depletion

(A) Immunophenotyping of NSCs and neuronal precursors called amplifying neural progenitors (ANP) that express nestin. Scale bar, 20μm.

(B) Nestin immunostaining in NTG and APP mice at 1, 2, and 6 to 7 months of age. Scale bar, 100 μm.

(C) The number of NSCs in NTG and APP mice at 1 (n = 10–11 mice per genotype), 2 (n = 14 mice per genotype), 3 (n = 8 mice per genotype), 6 (n = 9–10 mice per genotype), and 14 (n = 11–12 mice per genotype) months of age. Cell counts were normalized to the average of 1-month-old NTG mice.

(D) Immunophenotyping of dividing NSCs based on nestin expression and presence of BrdU. Scale bar, 20 μm.

(E) Nestin and BrdU staining in NTG and APP mice at 1, 2, and 6–7 months of age. Scale bar, 100 μm.

(F) The number of BrdU+ dividing NSCs in NTG and APP mice at 1 (n = 9–10 mice per genotype), 2 (n = 8 mice per genotype), 3 (n = 8 mice per genotype), 6 (n = 8 mice per genotype), and 14 (n = 11–12 mice per genotype) months of age. Cell counts were normalized to the average of 1-month-old NTG mice. Inset shows the proportion of dividing NSCs to total NSCs at the 2-month time point.

(G) Immunophenotyping of dividing NSCs based on nestin expression and presence of Ki67. Scale bar, 20 μm.

(H) Nestin and Ki67 staining in NTG and APP mice at 2 months of age. Scale bar, 50 μm.

(I) The total number of Ki67+ dividing NSCs in 2-month-old NTG and APP mice. Cell counts were normalized to the average of NTG mice (left; n = 8 mice per genotype). The percentage of dividing NSCs was calculated as the number of Ki67+ Nestin+ dividing NSCs divided by the total number of NSCs in NTG and APP mice (right).

*p < 0.05; **p < 0.01; ***p < 0.001; two-tailed unpaired Student's t test comparing means between NTG and APP mice at each age. Values indicate mean ± SEM. See also Figures S1, S3, S5, and S6 and Tables S1 and S2.

NSCs (Figures 3B and 3C). However, at 3 weeks of age, APP mice had more consecutively dividing NSCs compared to NTG mice, but fewer than NTG mice by 6 months of age (Figures 3B and 3C). These results were similar to the pattern found with just BrdU labeling (Figure 2F) and indicate that NSCs enter consecutive cycles of cell division in both APP and NTG mice. These data are compatible with the notion that the fundamental process of NSC division is not grossly altered in APP mice, but rather the rate at which they are engaged to enter the cell cycle.

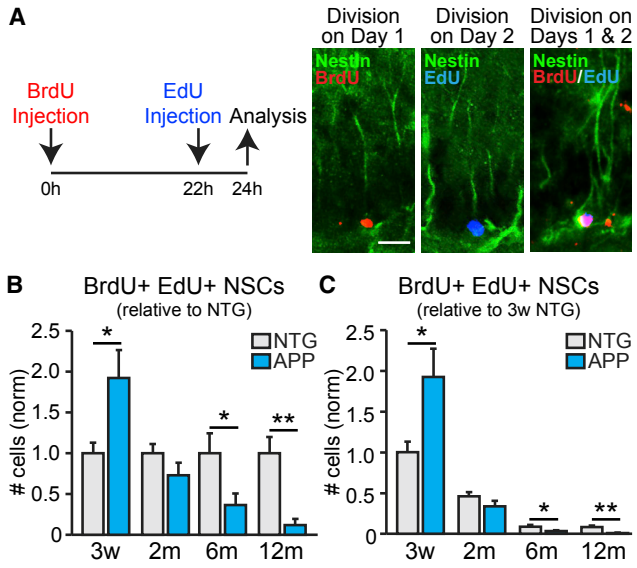

Figure 3. APP Mice Have Higher Fraction of NSCs Engaged in Consecutive Divisions Early in Life than NTG Mice Do

(A) Administration of BrdU and EdU 22 h apart captures NSCs that were dividing only on day 1 (BrdU+ NSCs), only on day 2 (EdU+ NSCs), or on both days 1 and 2 (BrdU+ EdU+ NSCs; "consecutively dividing NSCs"). Scale bar, 20 μm.

(B and C) Number of consecutively dividing NSCs at 3 weeks (n = 6 mice per genotype) and at 2 (n = 6–8 mice per genotype), 6 (n = 6–8 mice per genotype), and 12 (n = 5–8 mice per genotype) months of age, normalized to the average of the NTG mice at each time point (B) or 3-week-old NTG mice (C).

*p < 0.05; **p < 0.01; two-tailed unpaired Student's t test comparing means between NTG and APP mice at each age. Values indicate mean ± SEM. See also Figure S6 and Tables S1 and S2.

In support of this notion, when we challenged 8–10-month-old APP and NTG mice with a single injection of kainic acid (15 mg/kg), we found that although there are many fewer remaining NSCs in APP mice relative to NTG mice at this age, the kainic acid induced a proportionally similar increase in NSC division (Figure S6). This result suggests that the capacity of remaining NSCs to divide is unchanged in APP mice despite the accelerated depletion of the NSC pool.

Chronic Levetiracetam Treatment Normalizes Neurogenesis in APP Mice

One possible mechanism for the alterations in neurogenesis in APP mice is that the seizure activity that occurs early in disease progression aberrantly stimulates NSC division and accelerates depletion of the NSC pool (as in Figure 1A). In APP mice at 1 month of age, seizures are not obvious, but bursts of seizure-associated activity called interictal spikes or epileptiform activity do occur (see Figures 1B and 1D). By 2 months of age, APP mice exhibit robust seizures (see Figures 1C and 1D). To test if early seizure activity plays a causal role, we used the antiseizure drug levetiracetam (LEV), which effectively reduces spikes and seizures in APP mice (Corbett et al., 2017; Sanchez et al., 2012).

We previously found that a single injection of LEV (75 mg/kg) reduces epileptiform spikes in APP mice for up to 7 h and that 2 weeks of LEV treatment suppresses seizures (Corbett et al., 2017). We therefore treated 1.5-month-old APP and NTG mice with either LEV or saline (as a control) for 2 weeks. At this age, at which treatment was initiated, epileptiform spikes have begun in APP mice, but the number of NSCs was not yet altered (see Figures 1E–1G and 2A–2C).

Mice were sacrificed at the end of the 2-week treatment, when they were 2 months of age. The LEV efficacy was assessed by verifying that the expression of a seizure-induced transcription factor was reduced (Figure S7A; see Corbett et al., 2017). Similar to the naive APP mice described above, saline-treated APP mice had an increased proportion of dividing NSCs at 2 months of age, compared to saline-treated NTG mice (Figure 4A). However, this increase was prevented by the LEV treatment (Figure 4A). To test if the reduction in NSC division in the LEV-treated APP mice was sufficient to preserve the NSC pool, we assessed the total numbers of NSCs after LEV treatment. Saline-treated APP mice had fewer NSCs than NTG mice, as expected, but there was no difference in total NSCs between the LEV-treated APP and NTG mice (Figure 4B), suggesting a preservation of the NSC pool. These results demonstrate that chronic LEV treatment prevents the accelerated loss of NSCs in APP mice and normalizes the NSC pool. To assess whether LEV treatment also restored neurogenesis, we quantified DCX expression. At 2 months of age, saline-treated APP mice exhibited increased levels of DCX expression, compared to saline-treated NTG mice; this increase was prevented by the LEV treatment (Figure 4C). Taken together, these results suggest that reducing seizure activity in APP mice early in the disease progression can prevent or delay alterations in adult neurogenesis.

To test if the alterations in neurogenesis in APP mice might also be influenced by cell-autonomous processes in the NSCs, we prepared neurospheres from hippocampi of NTG and APP mice. NSCs from these neurospheres exhibited comparable rates of division from both NTG or APP mice (Figure S8). These results indicate that the alterations in neurogenesis and NSC dynamics in APP mice are unlikely to be due to cell-autonomous effects and suggest that the increases in NSC division early in the disease in APP mice was more likely due to circuit or network level factors, such as seizure activity.

Chronic LEV Treatment Improves Spatial Discrimination in APP Mice

Adult-born hippocampal neurons are critical for spatial discrimination (Aimone et al., 2011; Sahay et al., 2011). To determine whether spatial discrimination is impaired in APP mice—and, if so, whether restoring neurogenesis with LEV is sufficient to improve behavior—we used a spatial discrimination task modified from the object-location memory test (You et al., 2017). This spatial discrimination task assesses the ability of mice to distinguish incremental distances in object displacement (Figure 5A), which is dependent on the DG and contributes to the ability to discriminate between contexts (Danielson et al., 2016; Gonçalves et al., 2016).

We examined mice at 3–3.5 months of age, when the level of neurogenesis in APP mice first becomes markedly reduced

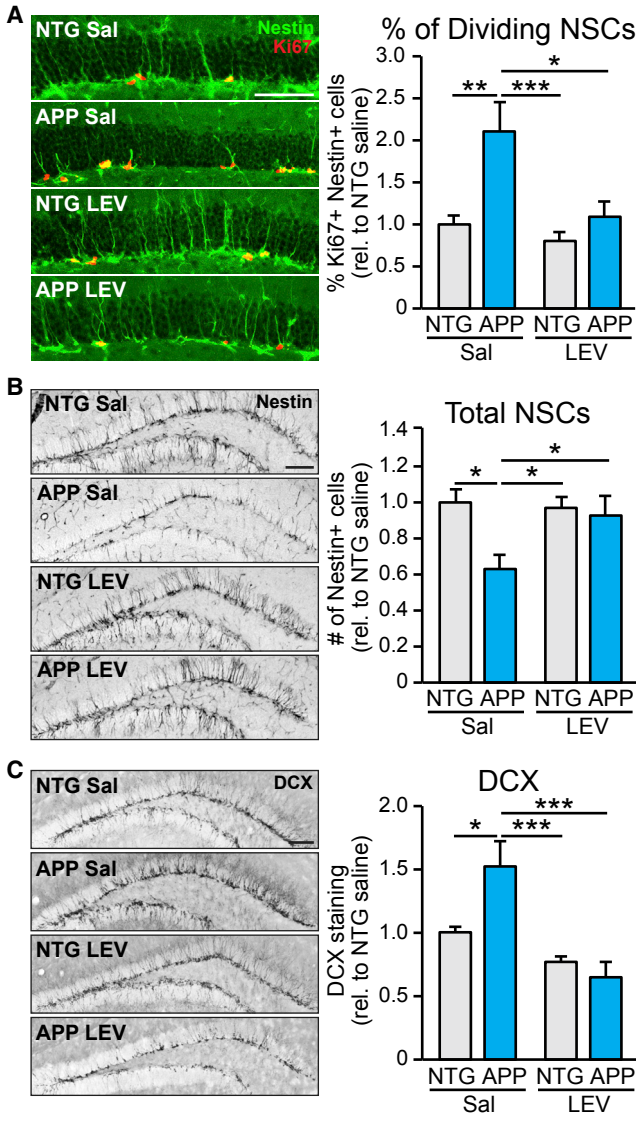

Figure 4. Chronic Levetiracetam Treatment Normalizes Neurogenesis in APP Mice

(A) After 2 weeks of treatment with saline or levetiracetam (LEV; 75 mg/kg), 2-month-old NTG and APP mice (n = 9–11 mice per genotype and treatment) were sacrificed, and the percentage of Ki67+ Nestin+ dividing NSCs was quantified. Two-way ANOVA: genotype ($p < 0.01$), treatment ($p < 0.05$). Scale bar, 100 μm.

(B) The total number of Nestin+ NSCs in NTG and APP mice treated with saline or LEV. Two-way ANOVA: genotype ($p < 0.05$), treatment and genotype interaction ($p < 0.05$). Scale bar, 100 μm.

(C) DCX expression in NTG and APP mice treated with saline or LEV. Two-way ANOVA: treatment ($p < 0.0001$), treatment and genotype interaction ($p < 0.05$). Scale bar, 100 μm.

*$p < 0.05$; **$p < 0.01$; ***$p < 0.001$; Holm–Sidak post hoc test. Values indicate mean ± SEM. See also Figures S7 and S8 and Tables S1 and S2.

compared to NTG controls (see Figure 1G). NTG mice were unable to discriminate a very short displacement distance (to position 1), as they spent roughly equal time exploring the displaced and nondisplaced objects. (Figure 5B). However, NTG mice spent more time with the displaced object when it was displaced to positions 2, 3, and 4, suggesting that they were able to discriminate those displacement distances. APP mice did not spend more time with the displaced object until it was displaced to position 3 (Figure 5B), indicating that a greater displacement is necessary for APP mice to discriminate changes in distance. Thus, the displacement distance to position 2 highlighted a key difference in discrimination ability between the NTG and APP mice. Indeed, the NTG mice spent more time exploring the displaced object at position 2 than did the APP mice (see Figures S9A and S9B).

To test if the LEV-induced restoration of neurogenesis dynamics in APP mice also improved their spatial discrimination ability, NTG and APP mice were treated with LEV or saline for 4 weeks via Alzet micro-osmotic pumps prior to spatial discrimination testing. This method of LEV administration effectively reduces epileptiform activity in APP mice (Figure S7; see also Sanchez et al., 2012) and reduced the expression of a seizure-induced transcription factor in the current study (Figures S7B–S7D). We implanted the micro-osmotic pumps into mice at just over 2 months of age and tested them at 3 months of age. Both saline- and LEV-treated NTG mice spent more time with the displaced object at position 2, whereas saline-treated APP mice did not, as expected (Figure 5C). Notably, the APP mice treated with LEV spent more time with the displaced object at position 2, indicating an improved spatial discrimination ability (Figure 5C). We noted that the time spent with the displaced object in the testing phase was slightly less in LEV-treated NTG mice than in saline-treated NTG mice (Figure 5C), so we calculated the spatial discrimination index for each group of mice and compared the magnitude of discrimination between groups. The LEV treatment did not affect the magnitude of spatial discrimination in the NTG mice, but it markedly improved the spatial discrimination of the APP mice (Figures S9C and S9D). These results do not prove that the improvement in spatial discrimination was due to the restoration of neurogenesis, but together they demonstrate that treatment of APP mice with an antiseizure drug restores neurogenesis dynamics and improves spatial discrimination.

DISCUSSION

We have shown that the hippocampal NSC pool in APP mice undergoes increased proliferation early in the disease progression, followed by accelerated age-dependent depletion. The early increase is associated with aberrant epileptiform activity, and the depletion is associated with the development of recurrent seizures.

This biphasic pattern of neurogenesis may help explain the divergent reports of the direction of change in neurogenesis in AD. Studies that found increased neurogenesis in AD generally investigated earlier stages of the disease progression, whereas those that found reduced neurogenesis generally examined later stages (Chevallier et al., 2005; Donovan et al., 2006; Hamilton et al., 2010; Jin et al., 2004a; Krezymon et al., 2013; López-Toledano and Shelanski, 2007; Rodríguez et al., 2008; Taniuchi et al., 2007; Unger et al., 2016; Verret et al., 2007; Zhang et al., 2007). A similar biphasic change in neurogenesis was previously

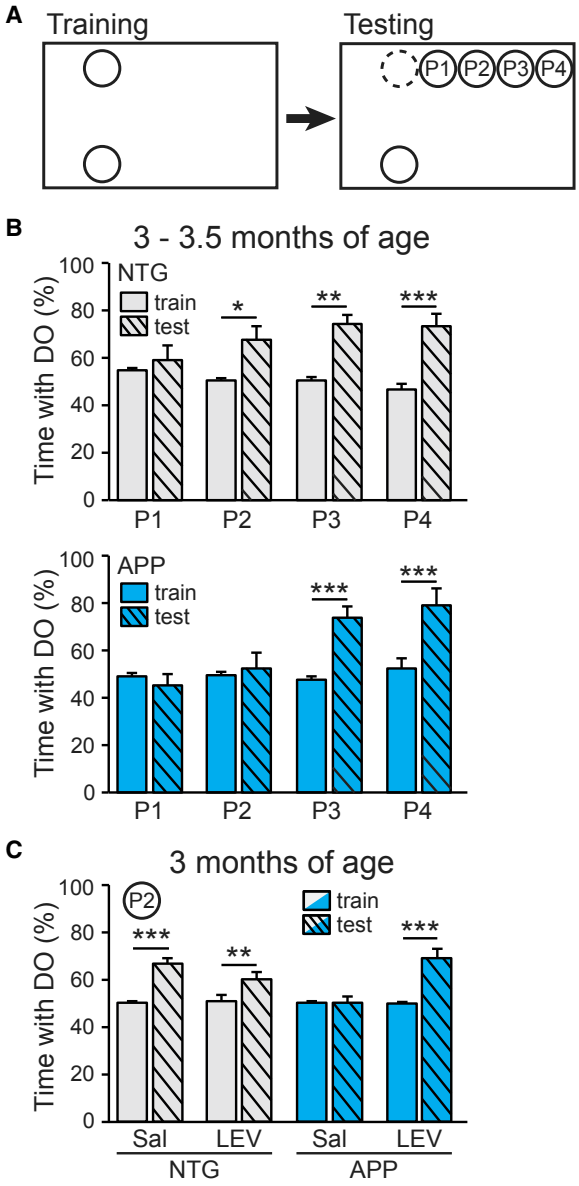

Figure 5. Chronic Levetiracetam Treatment Improves Spatial Discrimination in APP Mice

(A) Spatial discrimination task. Mice were trained with two identical objects placed on one side of cage, then tested with one object displaced to one of four positions (P1–P4).

(B) Percentage of time spent with the displaced object (DO) in 3–3.5-month-old NTG (top) and APP (bottom) mice at each of the four positions (P1, P2, P3, P4) during training and test trials (n = 6–8 mice per genotype and position, total 57 mice). NTG mice (top), two-way ANOVA: test phase ($p < 0.0001$), position and test phase interaction ($p < 0.001$). APP mice (bottom), two-way ANOVA: test position ($p < 0.01$), phase ($p < 0.001$), position and test phase interaction ($p < 0.001$).

(C) Percentage of time spent with the DO at P2 in 3-month-old NTG and APP mice after 4 weeks of treatment with saline or levetiracetam (n = 6–8 per genotype/treatment, total 30 mice). Two-way ANOVA: treatment ($p < 0.001$), test phase ($p < 0.0001$), treatment and test phase interaction ($p < 0.001$).

*$p < 0.05$; **$p < 0.01$; ***$p < 0.001$; Holm-Sidak post hoc test. Values indicate mean ± SEM. See also Figures S7 and S9 and Table S2.

found in the line of APP mice used in our studies, although the mechanism underlying such changes was not clear (López-Toledano and Shelanski, 2007). Notably, a recent study demonstrated that adult neurogenesis occurs throughout even the ninth decade of life in humans, and the extent of neurogenesis is diminished in individuals with AD (Moreno-Jiménez et al., 2019). Although the presence of seizures was not assessed in that study, it has been found in AD patients, as well as in numerous mouse models of AD as described previously, suggesting that alterations in neurogenesis described in those patients and models could potentially have been similarly affected by recurrent seizures. Indeed, non-monotonic alterations in neurogenesis with aging have been described in studies of aging mice, which supports the hypothesis that the neurogenic niche responds to changes in the local environment over time (Apostolopoulou et al., 2017).

Seizures appear to be intimately linked to alterations in neurogenesis and cognitive function both in AD and epilepsy. AD and epilepsy patients share many cognitive and psychiatric symptoms, pointing to possible common underlying mechanisms (Chin and Scharfman, 2013). Some of these overlapping symptoms, such as impairments in spatial discrimination and mood regulation, have both been associated with aberrant postnatal neurogenesis. Impairments in cognition and mood regulation are also observed in other diseases and disorders in which seizures have been reported, such as Parkinson's disease (Cooney and Stacy, 2016; Gruntz et al., 2018), Down syndrome (Menéndez, 2005), schizophrenia (Cascella et al., 2009), Rett syndrome (Chahrour and Zoghbi, 2007; Dolce et al., 2013), and others. It is therefore possible that any condition associated with recurrent seizures may similarly be affected by premature depletion of the hippocampal NSC pool, thus giving rise to similar cognitive and psychiatric symptoms.

Strategies that alter NSCs' fates and prevent them from exiting the pool after division may help preserve the NSC pool and function. To develop such strategies, it is necessary to understand what regulates NSCs as they go through the stages of division as well as entry and exit from the cell cycle. Some clues already exist. Using a combination of Nestin and Gli1 reporter lines, Encinas et al. (2011b) found that a population of NSCs did not self-renew, but instead underwent a few rapid asymmetric divisions to produce ANPs before terminally differentiating into astrocytes. A separate study using *in vivo* clonal analysis with Nestin-CreER^{T2} mice with Z-EG reporter to track NSCs did find evidence of self-renewal, however, underscoring the heterogeneity of NSCs in the DG (Bonaguidi et al., 2012, 2016, 2011). These studies focused on wild-type mice; it is not clear if these processes are regulated similarly in the context of disease. A recent study using an intrahippocampal kainic acid rodent model of temporal lobe epilepsy found that NSCs divide symmetrically before both mother and daughter cells convert into astrocytes, suggesting that the process can differ in at least some disease conditions (Sierra et al., 2015). Notably, using a weaker kainic acid stimulus that induces epileptiform spikes but not seizures, the authors did not find an increase in NSC conversion into astrocytes. Thus, heterogeneity exists not only in the ability of NSCs to renew themselves, but also in their fate after activation in different conditions. Alterations in long-range GABA-ergic

signaling may also contribute to varying effects on NSCs in different conditions, as impairments lead to increased NSC activation and subsequent depletion (Bao et al., 2017; Song et al., 2012). Additional therapeutic opportunities may lie in inducing remaining NSCs to self-renew and replenish the pool. Targeting the transcription factor REST may be beneficial, as its loss of function in induced pluripotent stem cells (iPSCs) derived from AD patients altered neural differentiation and depletion of NSCs (Meyer et al., 2019).

Our studies indicate that in APP mice, aberrant network activity is a primary driver of alterations in neurogenesis dynamics. Reducing epileptiform activity in APP mice normalized both neurogenesis and an associated behavior, whereas isolation and growth of NSCs from APP mice *in vitro* did not reveal altered dynamics in intrinsic cell division. These results do not preclude the possibility that APP or its cleavage products might yet have cell-autonomous effects on neurogenic processes, as reported (Lazarov and Demars, 2012). However, the robust effect of seizures on NSC division may overshadow other factors, or these factors may have differential impacts on NSC division, differentiation, or neuronal maturation.

Neurogenesis can also modulate network excitability. Newborn neurons promote inhibition in local hippocampal circuitry and may protect against neuronal injury after severe seizures (Drew et al., 2016; Iyengar et al., 2015; Jain et al., 2019). Thus, reduced neurogenesis in later stages of disease may exacerbate the excitation–inhibition imbalance. Seizures can also induce abnormalities in newborn neurons, such as mossy fiber sprouting, ectopic neuronal migration, and hilar basal dendrites, which may disrupt the circuitry and further promote seizures (Hester and Danzer, 2013; Jessberger et al., 2007). Additional studies are required to assess whether or how aberrant neurogenesis affects epileptogenesis in the APP mice in our study.

Neurogenesis is a multi-stage process that is influenced by many variables. Stimuli that affect neurogenesis may target distinct aspects of this process (Encinas et al., 2011a; Enikolopov et al., 2015; Lugert et al., 2010; Song et al., 2016). Deep brain stimulation in the anterior thalamic nucleus, physical exercise, and fluoxetine (Prozac) increase neurogenesis by stimulating the division of ANPs to increase neurogenic output (Encinas et al., 2011a, 2006), which is speculated to be how they exert their beneficial effects on cognition and mood. However, seizures and traumatic brain injuries also acutely increase neurogenesis but have negative long-term effects on function, which may be related to the fact that excitotoxic stimuli appear to activate the normally quiescent NSCs to divide (Gao et al., 2009; Lugert et al., 2010). Likewise, an ischemic brain injury, which initially induces a surge in NSC division in the subgranular zone (SGZ), ultimately leads to the long-term impairment of proliferation and neurogenesis (Lin et al., 2018). Our data suggest that a detrimental consequence of aberrantly activating quiescent NSCs is the premature exhaustion of a finite NSC pool. Treatment with antiepileptic drugs effectively controls seizures and restores the dynamics of neurogenesis, but is not necessarily optimal for long-term use due to possible adverse effects (Eddy et al., 2011; Schoenberg et al., 2017). Thus, therapeutic strategies to enhance neurogenesis may hold great promise for the treatment of cognitive and/or mood disorders, but care must be taken to stimulate the right cell types to increase neurogenic output but not deplete the NSC pool.

STAR★METHODS

Detailed methods are provided in the online version of this paper and include the following:

- KEY RESOURCES TABLE
- LEAD CONTACT AND MATERIALS AVAILABILITY
- EXPERIMENTAL MODEL AND SUBJECT DETAILS
- METHOD DETAILS
  - Immunohistochemistry
  - BrdU and EdU labeling
  - Neurosphere Experiments
  - EEG Recordings
  - Pharmacological Treatments
  - Spatial Discrimination Task
- QUANTIFICATION AND STATISTICAL ANALYSIS
  - Bias Elimination and Randomization
  - Statistical Analysis

SUPPLEMENTAL INFORMATION

Supplemental Information can be found online at https://doi.org/10.1016/j.celrep.2019.05.101.

ACKNOWLEDGMENTS

This work was supported by NIH grants NS086965 and NS085171 (J.C.), NS075839 (L.I.), NS086965 (H.E.S.), and AG040209 and NS086965 (G.E.) and by the New York State Office of Mental Health (H.E.S.).

AUTHOR CONTRIBUTIONS

C.-H.F., D.M.I., and J.C. conceived the study. C.-H.F., D.M.I., and J.L. performed the immunostaining and analyzed the data. M.S.P, U.T., and C.-H.F. performed behavioral testing. X.Z. and J.C. performed neurosphere assays. C.-H.F., D.M.I., I.P., A.H., U.T., B.F.C., and J.P. performed pharmacological treatments. I.P. and A.H. performed the electroencephalography. C.-H.F., D.M.I., X.Z., L.I., H.E.S., G.E., and J.C. designed and advised the experiments. C.-H.F., D.M.I., L.I., H.E.S., G.E., and J.C. wrote the paper. All authors reviewed and approved the manuscript.

DECLARATION OF INTERESTS

The authors declare no competing interests.

Received: May 3, 2018
Revised: April 24, 2019
Accepted: May 28, 2019
Published: June 25, 2019

REFERENCES

Aimone, J.B., Deng, W., and Gage, F.H. (2011). Resolving new memories: a critical look at the dentate gyrus, adult neurogenesis, and pattern separation. Neuron *70*, 589–596.

Aimone, J.B., Li, Y., Lee, S.W., Clemenson, G.D., Deng, W., and Gage, F.H. (2014). Regulation and function of adult neurogenesis: from genes to cognition. Physiol. Rev. *94*, 991–1026.

Ally, B.A., Hussey, E.P., Ko, P.C., and Molitor, R.J. (2013). Pattern separation and pattern completion in Alzheimer's disease: evidence of rapid

forgetting in amnestic mild cognitive impairment. Hippocampus *23*, 1246–1258.

Anacker, C., and Hen, R. (2017). Adult hippocampal neurogenesis and cognitive flexibility - linking memory and mood. Nat. Rev. Neurosci. *18*, 335–346.

Apostolopoulou, M., Kiehl, T.R., Winter, M., Cardenas De La Hoz, E., Boles, N.C., Bjornsson, C.S., Zuloaga, K.L., Goderie, S.K., Wang, Y., Cohen, A.R., and Temple, S. (2017). Non-monotonic Changes in Progenitor Cell Behavior and Gene Expression during Aging of the Adult V-SVZ Neural Stem Cell Niche. Stem Cell Rep. *9*, 1931–1947.

Bao, H., Asrican, B., Li, W., Gu, B., Wen, Z., Lim, S.A., Haniff, I., Ramakrishnan, C., Deisseroth, K., Philpot, B., et al. (2017). Long-Range GABAergic Inputs Regulate Neural Stem Cell Quiescence and Control Adult Hippocampal Neurogenesis. Cell Stem Cell *21*, 604–617.e605.

Bennett, L., Yang, M., Enikolopov, G., and Iacovitti, L. (2009). Circumventricular organs: a novel site of neural stem cells in the adult brain. Mol. Cell. Neurosci. *41*, 337–347.

Bergmann, O., Spalding, K.L., and Frisén, J. (2015). Adult Neurogenesis in Humans. Cold Spring Harb. Perspect. Biol. *7*, a018994.

Bertram, L., Lill, C.M., and Tanzi, R.E. (2010). The genetics of Alzheimer disease: back to the future. Neuron *68*, 270–281.

Boekhoorn, K., Joels, M., and Lucassen, P.J. (2006). Increased proliferation reflects glial and vascular-associated changes, but not neurogenesis in the presenile Alzheimer hippocampus. Neurobiol. Dis. *24*, 1–14.

Boldrini, M., Fulmore, C.A., Tartt, A.N., Simeon, L.R., Pavlova, I., Poposka, V., Rosoklija, G.B., Stankov, A., Arango, V., Dwork, A.J., et al. (2018). Human Hippocampal Neurogenesis Persists throughout Aging. Cell Stem Cell *22*, 589–599.e585.

Bonaguidi, M.A., Wheeler, M.A., Shapiro, J.S., Stadel, R.P., Sun, G.J., Ming, G.L., and Song, H. (2011). In vivo clonal analysis reveals self-renewing and multipotent adult neural stem cell characteristics. Cell *145*, 1142–1155.

Bonaguidi, M.A., Song, J., Ming, G.L., and Song, H. (2012). A unifying hypothesis on mammalian neural stem cell properties in the adult hippocampus. Curr. Opin. Neurobiol. *22*, 754–761.

Bonaguidi, M.A., Stadel, R.P., Berg, D.A., Sun, J., Ming, G.L., and Song, H. (2016). Diversity of Neural Precursors in the Adult Mammalian Brain. Cold Spring Harb. Perspect. Biol. *8*, a018838.

Briley, D., Ghirardi, V., Woltjer, R., Renck, A., Zolochevska, O., Taglialatela, G., and Micci, M.A. (2016). Preserved neurogenesis in non-demented individuals with AD neuropathology. Sci. Rep. *6*, 27812.

Cascella, N.G., Schretlen, D.J., and Sawa, A. (2009). Schizophrenia and epilepsy: is there a shared susceptibility? Neurosci. Res. *63*, 227–235.

Chahrour, M., and Zoghbi, H.Y. (2007). The story of Rett syndrome: from clinic to neurobiology. Neuron *56*, 422–437.

Chevallier, N.L., Soriano, S., Kang, D.E., Masliah, E., Hu, G., and Koo, E.H. (2005). Perturbed neurogenesis in the adult hippocampus associated with presenilin-1 A246E mutation. Am. J. Pathol. *167*, 151–159.

Chin, J., and Scharfman, H.E. (2013). Shared cognitive and behavioral impairments in epilepsy and Alzheimer's disease and potential underlying mechanisms. Epilepsy Behav. *26*, 343–351.

Christian, K.M., Song, H., and Ming, G.L. (2014). Functions and dysfunctions of adult hippocampal neurogenesis. Annu. Rev. Neurosci. *37*, 243–262.

Cooney, J.W., and Stacy, M. (2016). Neuropsychiatric Issues in Parkinson's Disease. Curr. Neurol. Neurosci. Rep. *16*, 49.

Corbett, B.F., You, J.C., Zhang, X., Pyfer, M.S., Tosi, U., Iascone, D.M., Petrof, I., Hazra, A., Fu, C.-H., Stephens, G.S., et al. (2017). ΔFosB Regulates Gene Expression and Cognitive Dysfunction in a Mouse Model of Alzheimer's Disease. Cell Rep. *20*, 344–355.

Danielson, N.B., Kaifosh, P., Zaremba, J.D., Lovett-Barron, M., Tsai, J., Denny, C.A., Balough, E.M., Goldberg, A.R., Drew, L.J., Hen, R., et al. (2016). Distinct contribution of adult-born hippocampal granule cells to context encoding. Neuron *90*, 101–112.

Dolce, A., Ben-Zeev, B., Naidu, S., and Kossoff, E.H. (2013). Rett syndrome and epilepsy: an update for child neurologists. Pediatr. Neurol. *48*, 337–345.

Donovan, M.H., Yazdani, U., Norris, R.D., Games, D., German, D.C., and Eisch, A.J. (2006). Decreased adult hippocampal neurogenesis in the PDAPP mouse model of Alzheimer's disease. J. Comp. Neurol. *495*, 70–83.

Drew, L.J., Kheirbek, M.A., Luna, V.M., Denny, C.A., Cloidt, M.A., Wu, M.V., Jain, S., Scharfman, H.E., and Hen, R. (2016). Activation of local inhibitory circuits in the dentate gyrus by adult-born neurons. Hippocampus *26*, 763–778.

Eddy, C.M., Rickards, H.E., and Cavanna, A.E. (2011). The cognitive impact of antiepileptic drugs. Ther. Adv. Neurol. Disorder. *4*, 385–407.

Encinas, J.M., and Enikolopov, G. (2008). Identifying and quantitating neural stem and progenitor cells in the adult brain. Methods Cell Biol. *85*, 243–272.

Encinas, J.M., Vaahtokari, A., and Enikolopov, G. (2006). Fluoxetine targets early progenitor cells in the adult brain. Proc. Natl. Acad. Sci. USA *103*, 8233–8238.

Encinas, J.M., Hamani, C., Lozano, A.M., and Enikolopov, G. (2011a). Neurogenic hippocampal targets of deep brain stimulation. J. Comp. Neurol. *519*, 6–20.

Encinas, J.M., Michurina, T.V., Peunova, N., Park, J.H., Tordo, J., Peterson, D.A., Fishell, G., Koulakov, A., and Enikolopov, G. (2011b). Division-coupled astrocytic differentiation and age-related depletion of neural stem cells in the adult hippocampus. Cell Stem Cell. *8*, 566–579.

Enikolopov, G., Overstreet-Wadiche, L., and Ge, S. (2015). Viral and transgenic reporters and genetic analysis of adult neurogenesis. Cold Spring Harb. Perspect. Biol. *7*, a018804.

Eriksson, P.S., Perfilieva, E., Björk-Eriksson, T., Alborn, A.M., Nordborg, C., Peterson, D.A., and Gage, F.H. (1998). Neurogenesis in the adult human hippocampus. Nat. Med. *4*, 1313–1317.

Ernst, A., Alkass, K., Bernard, S., Salehpour, M., Perl, S., Tisdale, J., Possnert, G., Druid, H., and Frisén, J. (2014). Neurogenesis in the striatum of the adult human brain. Cell *156*, 1072–1083.

Fjell, A.M., McEvoy, L., Holland, D., Dale, A.M., and Walhovd, K.B.; Alzheimer's Disease Neuroimaging Initiative (2014). What is normal in normal aging? Effects of aging, amyloid and Alzheimer's disease on the cerebral cortex and the hippocampus. Prog. Neurobiol. *117*, 20–40.

Gao, X., Enikolopov, G., and Chen, J. (2009). Moderate traumatic brain injury promotes proliferation of quiescent neural progenitors in the adult hippocampus. Exp. Neurol. *219*, 516–523.

Gonçalves, J.T., Schafer, S.T., and Gage, F.H. (2016). Adult Neurogenesis in the Hippocampus: From Stem Cells to Behavior. Cell *167*, 897–914.

Gray, W.P., and Sundstrom, L.E. (1998). Kainic acid increases the proliferation of granule cell progenitors in the dentate gyrus of the adult rat. Brain Res. *790*, 52–59.

Gruntz, K., Bloechliger, M., Becker, C., Jick, S.S., Fuhr, P., Meier, C.R., and Rüegg, S. (2018). Parkinson disease and the risk of epileptic seizures. Ann. Neurol. *83*, 363–374.

Hamilton, L.K., Aumont, A., Julien, C., Vadnais, A., Calon, F., and Fernandes, K.J. (2010). Widespread deficits in adult neurogenesis precede plaque and tangle formation in the 3xTg mouse model of Alzheimer's disease. Eur. J. Neurosci. *32*, 905–920.

Hattiangady, B., Rao, M.S., and Shetty, A.K. (2004). Chronic temporal lobe epilepsy is associated with severely declined dentate neurogenesis in the adult hippocampus. Neurobiol. Dis. *17*, 473–490.

Haughey, N.J., Nath, A., Chan, S.L., Borchard, A.C., Rao, M.S., and Mattson, M.P. (2002). Disruption of neurogenesis by amyloid beta-peptide, and perturbed neural progenitor cell homeostasis, in models of Alzheimer's disease. J. Neurochem. *83*, 1509–1524.

Hauser, W.A., Morris, M.L., Heston, L.L., and Anderson, V.E. (1986). Seizures and myoclonus in patients with Alzheimer's disease. Neurology *36*, 1226–1230.

Hester, M.S., and Danzer, S.C. (2013). Accumulation of abnormal adult-generated hippocampal granule cells predicts seizure frequency and severity. J. Neurosci. *33*, 8926–8936.

Holcomb, L., Gordon, M.N., McGowan, E., Yu, X., Benkovic, S., Jantzen, P., Wright, K., Saad, I., Mueller, R., Morgan, D., et al. (1998). Accelerated Alzheimer-type phenotype in transgenic mice carrying both mutant amyloid precursor protein and presenilin 1 transgenes. Nat. Med. *4*, 97–100.

Holtzman, D.M., Morris, J.C., and Goate, A.M. (2011). Alzheimer's disease: the challenge of the second century. Sci. Transl. Med. *3*, 77sr1.

Hsiao, K., Chapman, P., Nilsen, S., Eckman, C., Harigaya, Y., Younkin, S., Yang, F., and Cole, G. (1996). Correlative memory deficits, Abeta elevation, and amyloid plaques in transgenic mice. Science *274*, 99–102.

Iyengar, S.S., LaFrancois, J.J., Friedman, D., Drew, L.J., Denny, C.A., Burghardt, N.S., Wu, M.V., Hsieh, J., Hen, R., and Scharfman, H.E. (2015). Suppression of adult neurogenesis increases the acute effects of kainic acid. Exp. Neurol. *264*, 135–149.

Jain, S., LaFrancois, J.J., Botterill, J.J., Alcantara-Gonzalez, D., and Scharfman, H.E. (2019). Adult neurogenesis in the mouse dentate gyrus protects the hippocampus from neuronal injury following severe seizures. Hippocampus, Published online January 23, 2019. https://doi.org/10.1002/hipo.23062.

Jessberger, S., Zhao, C., Toni, N., Clemenson, G.D., Jr., Li, Y., and Gage, F.H. (2007). Seizure-associated, aberrant neurogenesis in adult rats characterized with retrovirus-mediated cell labeling. J. Neurosci. *27*, 9400–9407.

Jin, K., Galvan, V., Xie, L., Mao, X.O., Gorostiza, O.F., Bredesen, D.E., and Greenberg, D.A. (2004a). Enhanced neurogenesis in Alzheimer's disease transgenic (PDGF-APPSw,Ind) mice. Proc. Natl. Acad. Sci. USA *101*, 13363–13367.

Jin, K., Peel, A.L., Mao, X.O., Xie, L., Cottrell, B.A., Henshall, D.C., and Greenberg, D.A. (2004b). Increased hippocampal neurogenesis in Alzheimer's disease. Proc. Natl. Acad. Sci. USA *101*, 343–347.

Kam, K., Duffy, A.M., Moretto, J., LaFrancois, J.J., and Scharfman, H.E. (2016). Interictal spikes during sleep are an early defect in the Tg2576 mouse model of β-amyloid neuropathology. Sci. Rep. *6*, 20119.

Kempermann, G., Gage, F.H., Aigner, L., Song, H., Curtis, M.A., Thuret, S., Kuhn, H.G., Jessberger, S., Frankland, P.W., Cameron, H.A., et al. (2018). Human Adult Neurogenesis: Evidence and Remaining Questions. Cell Stem Cell *23*, 25–30.

Kheirbek, M.A., Drew, L.J., Burghardt, N.S., Costantini, D.O., Tannenholz, L., Ahmari, S.E., Zeng, H., Fenton, A.A., and Hen, R. (2013). Differential control of learning and anxiety along the dorsoventral axis of the dentate gyrus. Neuron *77*, 955–968.

Knoth, R., Singec, I., Ditter, M., Pantazis, G., Capetian, P., Meyer, R.P., Horvat, V., Volk, B., and Kempermann, G. (2010). Murine features of neurogenesis in the human hippocampus across the lifespan from 0 to 100 years. PLoS ONE *5*, e8809.

Krezymon, A., Richetin, K., Halley, H., Roybon, L., Lassalle, J.M., Francès, B., Verret, L., and Rampon, C. (2013). Modifications of hippocampal circuits and early disruption of adult neurogenesis in the tg2576 mouse model of Alzheimer's disease. PLoS ONE *8*, e76497.

Lam, A.D., Deck, G., Goldman, A., Eskandar, E.N., Noebels, J., and Cole, A.J. (2017). Silent hippocampal seizures and spikes identified by foramen ovale electrodes in Alzheimer's disease. Nat. Med. *23*, 678–680.

Lazarov, O., and Demars, M.P. (2012). All in the Family: How the APPs Regulate Neurogenesis. Front. Neurosci. *6*, 81.

Leal, S.L., and Yassa, M.A. (2013). Perturbations of neural circuitry in aging, mild cognitive impairment, and Alzheimer's disease. Ageing Res. Rev. *12*, 823–831.

Ledergerber, D., Fritschy, J.M., and Kralic, J.E. (2006). Impairment of dentate gyrus neuronal progenitor cell differentiation in a mouse model of temporal lobe epilepsy. Exp. Neurol. *199*, 130–142.

Lin, R., Lang, M., Heinsinger, N., Stricsek, G., Zhang, J., Iozzo, R., Rosenwasser, R., and Iacovitti, L. (2018). Stepwise impairment of neural stem cell proliferation and neurogenesis concomitant with disruption of blood-brain barrier in recurrent ischemic stroke. Neurobiol. Dis. *115*, 49–58.

López-Toledano, M.A., and Shelanski, M.L. (2007). Increased neurogenesis in young transgenic mice overexpressing human APP(Sw, Ind). J. Alzheimers Dis. *12*, 229–240.

Lozsadi, D.A., and Larner, A.J. (2006). Prevalence and causes of seizures at the time of diagnosis of probable Alzheimer's disease. Dement. Geriatr. Cogn. Disord. *22*, 121–124.

Lugert, S., Basak, O., Knuckles, P., Haussler, U., Fabel, K., Götz, M., Haas, C.A., Kempermann, G., Taylor, V., and Giachino, C. (2010). Quiescent and active hippocampal neural stem cells with distinct morphologies respond selectively to physiological and pathological stimuli and aging. Cell Stem Cell. *6*, 445–456.

Menéndez, M. (2005). Down syndrome, Alzheimer's disease and seizures. Brain Dev. *27*, 246–252.

Meyer, K., Feldman, H.M., Lu, T., Drake, D., Lim, E.T., Ling, K.H., Bishop, N.A., Pan, Y., Seo, J., Lin, Y.T., et al. (2019). REST and Neural Gene Network Dysregulation in iPSC Models of Alzheimer's Disease. Cell Rep. *26*, 1112–1127.e1119.

Miller, B.R., and Hen, R. (2015). The current state of the neurogenic theory of depression and anxiety. Curr. Opin. Neurobiol. *30*, 51–58.

Minkeviciene, R., Rheims, S., Dobszay, M.B., Zilberter, M., Hartikainen, J., Fülöp, L., Penke, B., Zilberter, Y., Harkany, T., Pitkänen, A., and Tanila, H. (2009). Amyloid beta-induced neuronal hyperexcitability triggers progressive epilepsy. J. Neurosci. *29*, 3453–3462.

Moreno-Jiménez, E.P., Flor-García, M., Terreros-Roncal, J., Rábano, A., Cafini, F., Pallas-Bazarra, N., Ávila, J., and Llorens-Martín, M. (2019). Adult hippocampal neurogenesis is abundant in neurologically healthy subjects and drops sharply in patients with Alzheimer's disease. Nat. Med. *25*, 554–560.

Morrison, J.H., and Hof, P.R. (2002). Selective vulnerability of corticocortical and hippocampal circuits in aging and Alzheimer's disease. Prog. Brain Res. *136*, 467–486.

Mu, Y., and Gage, F.H. (2011). Adult hippocampal neurogenesis and its role in Alzheimer's disease. Mol. Neurodegener. *6*, 85.

Mucke, L., and Selkoe, D.J. (2012). Neurotoxicity of amyloid β-protein: synaptic and network dysfunction. Cold Spring Harb. Perspect. Med. *2*, a006338.

Mucke, L., Masliah, E., Yu, G.Q., Mallory, M., Rockenstein, E.M., Tatsuno, G., Hu, K., Kholodenko, D., Johnson-Wood, K., and McConlogue, L. (2000). High-level neuronal expression of abeta 1-42 in wild-type human amyloid protein precursor transgenic mice: synaptotoxicity without plaque formation. J. Neurosci. *20*, 4050–4058.

Myers, C.E., Bermudez-Hernandez, K., and Scharfman, H.E. (2013). The influence of ectopic migration of granule cells into the hilus on dentate gyrus-CA3 function. PLoS ONE *8*, e68208.

Nakagawa, E., Aimi, Y., Yasuhara, O., Tooyama, I., Shimada, M., McGeer, P.L., and Kimura, H. (2000). Enhancement of progenitor cell division in the dentate gyrus triggered by initial limbic seizures in rat models of epilepsy. Epilepsia *41*, 10–18.

Nakashiba, T., Cushman, J.D., Pelkey, K.A., Renaudineau, S., Buhl, D.L., McHugh, T.J., Rodriguez Barrera, V., Chittajallu, R., Iwamoto, K.S., McBain, C.J., et al. (2012). Young dentate granule cells mediate pattern separation, whereas old granule cells facilitate pattern completion. Cell *149*, 188–201.

Palop, J.J., Chin, J., Roberson, E.D., Wang, J., Thwin, M.T., Bien-Ly, N., Yoo, J., Ho, K.O., Yu, G.Q., Kreitzer, A., et al. (2007). Aberrant excitatory neuronal activity and compensatory remodeling of inhibitory hippocampal circuits in mouse models of Alzheimer's disease. Neuron *55*, 697–711.

Parent, J.M. (2007). Adult neurogenesis in the intact and epileptic dentate gyrus. Prog. Brain Res. *163*, 529–540.

Parent, J.M., Elliott, R.C., Pleasure, S.J., Barbaro, N.M., and Lowenstein, D.H. (2006). Aberrant seizure-induced neurogenesis in experimental temporal lobe epilepsy. Ann. Neurol. *59*, 81–91.

Pilz, G.A., Bottes, S., Betizeau, M., Jörg, D.J., Carta, S., Simons, B.D., Helmchen, F., and Jessberger, S. (2018). Live imaging of neurogenesis in the adult mouse hippocampus. Science *359*, 658–662.

Richetin, K., Leclerc, C., Toni, N., Gallopin, T., Pech, S., Roybon, L., and Rampon, C. (2015). Genetic manipulation of adult-born hippocampal neurons rescues memory in a mouse model of Alzheimer's disease. Brain *138*, 440–455.

Rodríguez, J.J., and Verkhratsky, A. (2011). Neurogenesis in Alzheimer's disease. J. Anat. *219*, 78–89.

Rodríguez, J.J., Jones, V.C., Tabuchi, M., Allan, S.M., Knight, E.M., LaFerla, F.M., Oddo, S., and Verkhratsky, A. (2008). Impaired adult neurogenesis in the dentate gyrus of a triple transgenic mouse model of Alzheimer's disease. PLoS ONE *3*, e2935.

Sahay, A., Scobie, K.N., Hill, A.S., O'Carroll, C.M., Kheirbek, M.A., Burghardt, N.S., Fenton, A.A., Dranovsky, A., and Hen, R. (2011). Increasing adult hippocampal neurogenesis is sufficient to improve pattern separation. Nature *472*, 466–470.

Sala, M., Perez, J., Soloff, P., Ucelli di Nemi, S., Caverzasi, E., Soares, J.C., and Brambilla, P. (2004). Stress and hippocampal abnormalities in psychiatric disorders. Eur. Neuropsychopharmacol. *14*, 393–405.

Salmon, D.P. (2012). Neuropsychological features of mild cognitive impairment and preclinical Alzheimer's disease. In Behavioral Neurobiology of Aging, M.-C. Pardon and M.W. Bondi, eds. (Springer Berlin Heidelberg), pp. 187–212.

Sanchez, P.E., Zhu, L., Verret, L., Vossel, K.A., Orr, A.G., Cirrito, J.R., Devidze, N., Ho, K., Yu, G.Q., Palop, J.J., and Mucke, L. (2012). Levetiracetam suppresses neuronal network dysfunction and reverses synaptic and cognitive deficits in an Alzheimer's disease model. Proc. Natl. Acad. Sci. USA *109*, E2895–E2903.

Scarmeas, N., Honig, L.S., Choi, H., Cantero, J., Brandt, J., Blacker, D., Albert, M., Amatniek, J.C., Marder, K., Bell, K., et al. (2009). Seizures in Alzheimer disease: who, when, and how common? Arch. Neurol. *66*, 992–997.

Scharfman, H.E., and Gray, W.P. (2007). Relevance of seizure-induced neurogenesis in animal models of epilepsy to the etiology of temporal lobe epilepsy. Epilepsia *48*, 33–41.

Scharfman, H.E., Goodman, J.H., and Sollas, A.L. (2000). Granule-like neurons at the hilar/CA3 border after status epilepticus and their synchrony with area CA3 pyramidal cells: functional implications of seizure-induced neurogenesis. J. Neurosci. *20*, 6144–6158.

Schoenberg, M.R., Rum, R.S., Osborn, K.E., and Werz, M.A. (2017). A randomized, double-blind, placebo-controlled crossover study of the effects of levetiracetam on cognition, mood, and balance in healthy older adults. Epilepsia *58*, 1566–1574.

Sierra, A., Martín-Suárez, S., Valcárcel-Martín, R., Pascual-Brazo, J., Aelvoet, S.A., Abiega, O., Deudero, J.J., Brewster, A.L., Bernales, I., Anderson, A.E., et al. (2015). Neuronal hyperactivity accelerates depletion of neural stem cells and impairs hippocampal neurogenesis. Cell Stem Cell *16*, 488–503.

Song, J., Zhong, C., Bonaguidi, M.A., Sun, G.J., Hsu, D., Gu, Y., Meletis, K., Huang, Z.J., Ge, S., Enikolopov, G., et al. (2012). Neuronal circuitry mechanism regulating adult quiescent neural stem-cell fate decision. Nature *489*, 150–154.

Song, J., Olsen, R.H., Sun, J., Ming, G.L., and Song, H. (2016). Neuronal Circuitry Mechanisms Regulating Adult Mammalian Neurogenesis. Cold Spring Harb. Perspect. Biol. *8*, a018937.

Sorrells, S.F., Paredes, M.F., Cebrian-Silla, A., Sandoval, K., Qi, D., Kelley, K.W., James, D., Mayer, S., Chang, J., Auguste, K.I., et al. (2018). Human hippocampal neurogenesis drops sharply in children to undetectable levels in adults. Nature *555*, 377–381.

Sotthibundhu, A., Li, Q.X., Thangnipon, W., and Coulson, E.J. (2009). Abeta(1-42) stimulates adult SVZ neurogenesis through the p75 neurotrophin receptor. Neurobiol. Aging *30*, 1975–1985.

Spalding, K.L., Bergmann, O., Alkass, K., Bernard, S., Salehpour, M., Huttner, H.B., Boström, E., Westerlund, I., Vial, C., Buchholz, B.A., et al. (2013). Dynamics of hippocampal neurogenesis in adult humans. Cell *153*, 1219–1227.

Taniuchi, N., Niidome, T., Goto, Y., Akaike, A., Kihara, T., and Sugimoto, H. (2007). Decreased proliferation of hippocampal progenitor cells in APPswe/PS1dE9 transgenic mice. Neuroreport. *18*, 1801–1805.

Unger, M.S., Marschallinger, J., Kaindl, J., Höfling, C., Rossner, S., Heneka, M.T., Van der Linden, A., and Aigner, L. (2016). Early Changes in Hippocampal Neurogenesis in Transgenic Mouse Models for Alzheimer's Disease. Mol. Neurobiol. *53*, 5796–5806.

Verret, L., Jankowsky, J.L., Xu, G.M., Borchelt, D.R., and Rampon, C. (2007). Alzheimer's-type amyloidosis in transgenic mice impairs survival of newborn neurons derived from adult hippocampal neurogenesis. J. Neurosci. *27*, 6771–6780.

Vossel, K.A., Beagle, A.J., Rabinovici, G.D., Shu, H., Lee, S.E., Naasan, G., Hegde, M., Cornes, S.B., Henry, M.L., Nelson, A.B., et al. (2013). Seizures and epileptiform activity in the early stages of Alzheimer disease. JAMA Neurol. *70*, 1158–1166.

Vossel, K.A., Ranasinghe, K.G., Beagle, A.J., Mizuiri, D., Honma, S.M., Dowling, A.F., Darwish, S.M., Van Berlo, V., Barnes, D.E., Mantle, M., et al. (2016). Incidence and impact of subclinical epileptiform activity in Alzheimer's disease. Ann. Neurol. *80*, 858–870.

Weintraub, S., Wicklund, A.H., and Salmon, D.P. (2012). The neuropsychological profile of Alzheimer disease. Cold Spring Harb. Perspect. Med. *2*, a006171.

Wesnes, K.A., Annas, P., Basun, H., Edgar, C., and Blennow, K. (2014). Performance on a pattern separation task by Alzheimer's patients shows possible links between disrupted dentate gyrus activity and apolipoprotein E ε4 status and cerebrospinal fluid amyloid-β42 levels. Alzheimers Res. Ther. *6*, 20.

Wimmer, M.E., Hernandez, P.J., Blackwell, J., and Abel, T. (2012). Aging impairs hippocampus-dependent long-term memory for object location in mice. Neurobiol. Aging *33*, 2220–2224.

You, J.C., Muralidharan, K., Park, J.W., Petrof, I., Pyfer, M.S., Corbett, B.F., LaFrancois, J.J., Zheng, Y., Zhang, X., Mohila, C.A., et al. (2017). Epigenetic suppression of hippocampal calbindin-D28k by ΔFosB drives seizure-related cognitive deficits. Nat. Med. *23*, 1377–1383.

Zhang, C., McNeil, E., Dressler, L., and Siman, R. (2007). Long-lasting impairment in hippocampal neurogenesis associated with amyloid deposition in a knock-in mouse model of familial Alzheimer's disease. Exp. Neurol. *204*, 77–87.

STAR★METHODS

KEY RESOURCES TABLE

REAGENT or RESOURCE	SOURCE	IDENTIFIER
Antibodies		
Rabbit anti-doublecortin	Cell Signaling Technologies	Cat# 4604; RRID: AB_561007
Mouse anti-nestin	Millipore-Sigma	Cat# MAB353; RRID: AB_94911
Chicken anti-nestin	Novus Biologicals	Cat# NB100-1604; RRID: AB_2282642
Rat anti-BrdU	Accurate Chemical	Cat# OBT0030G; RRID: AB_609567
Mouse anti-BrdU	Sigma-Aldrich	Cat# B8434; RRID: AB_476811
Rabbit anti-Ki67	ThermoFisher Scientific	Cat# RM-9106-S1; RRID: AB_149792
Mouse anti-PSA-NCAM	Millipore-Sigma	Cat# MAB5324; RRID: AB_95211
Rabbit anti-β3-tubulin	Cell Signaling Technologies	Cat#: 5568; RRID: AB_10694505
Mouse anti-Prox1	PhosphoSolutions	Cat#: 1685-Prox1; RRID: AB_2492217
Rabbit anti-ΔFosB	Cell Signaling Technologies	Cat#: 14695; RRID: AB_2798577
Chemicals, Peptides, and Recombinant Proteins		
5-bromo-2′-deoxyuridine (BrdU)	Sigma-Aldrich	Cat# B5002
5-ethynyl-2′-deoxyuridine (EdU)	Invitrogen	Cat# A10044
Kainic acid	Sigma-Aldrich	Cat# K0250-10MG
3,3-diaminobenzidine (DAB)	Sigma-Aldrich	Cat# D5905-50TAB
Levetiracetam	Sequoia Research Products	Cat# SRP013811
Papain	Roche	Cat# 10108014001
DNaseI	Roche	Cat# 04716728001
L-cystein	Sigma-Aldrich	Cat# C7352
bFGF	R&D Systems	Cat# P15655
EGF	R&D Systems	Cat# 2028-EG
Heparin Sodium	Sigma-Aldrich	Cat# H4784
N2 supplement	Invitrogen	Cat# 17502048
B27 supplement	Invitrogen	Cat# 17504044
Geltrex	Invitrogen	Cat# A1413302
Critical Commercial Assays		
Click-iT EdU Alexa Fluor 647 Imaging Kit	Invitrogen	Cat# C10340
Experimental Models: Organisms/Strains		
B6.Cg-Zbtb20Tg(PDGFB-APPSwInd)20Lms/2Mmjax (J20)	The Jackson Laboratory	MMRRC stock #34836
Software and Algorithms		
Prism 6	GraphPad	https://www.graphpad.com/scientific-software/prism/; RRID: SCR_002798
MetaMorph software	Molecular Devices	https://www.moleculardevices.com/systems/metamorph-research-imaging/metamorph-microscopy-automation-and-image-analysis-software; RRID:SCR_002368
ZEN software	Zeiss Microscope	https://www.zeiss.com/microscopy/int/products/microscope-software/zen.html; RRID: SCR_013672
FIJI (ImageJ)	NIH	RRID: SCR_002285

(*Continued on next page*)

Continued

REAGENT or RESOURCE	SOURCE	IDENTIFIER
Adobe Illustrator CC	Adobe	http://www.adobe.com/products/illustrator.html; RRID: SCR_010279
Adobe Photoshop CC	Adobe	https://www.adobe.com/products/photoshop.html; RRID: SCR_014199
Other		
Micro-osmotic pump	Alzet Osmotic Pumps	Model 1004

LEAD CONTACT AND MATERIALS AVAILABILITY

Further information and requests for resources and reagents should be directed to and will be fulfilled by the Lead Contact, Jeannie Chin (Jeannie.Chin@bcm.edu).

EXPERIMENTAL MODEL AND SUBJECT DETAILS

Heterozygous transgenic mice (line J20) expressing human amyloid precursor protein (APP) carrying Swedish (K670N, M671L) and Indiana (V717F) familial AD (FAD) mutations (hAPP770 numbering) were used in this study (Mucke et al., 2000). Transgene expression in this line is directed by the platelet-derived growth factor β chain promoter. This line has been crossed for > 10 generations onto a C57BL/6J background using nontransgenic (NTG) C57BL/6J mice from The Jackson Laboratory (Bar Harbor, ME). APP mice are bred, maintained, and analyzed as heterozygous transgenic mice, and age-matched NTG littermates from the same line are used as controls. Male and female mice between the ages of 3 weeks old to 14 months old were used; see Figure Legends for the specific ages used in each figure. Mice are housed in group-housing with *ad libitum* access to food and water, and maintained on a regular 12/12 light/dark cycle. No specific method of randomization was used, but mice were semirandomly assigned to experimental groups on the basis of birth order after balancing for age, sex, and genotype. No sex differences were observed. Experiments were performed by investigators who were blinded to the genotype and treatment of the mice. For harvesting of brains, mice were deeply anesthetized and flush-perfused transcardially with phosphate-buffered saline. Brains were post-fixed in 4% phosphate-buffered paraformaldehyde. All experiments were approved by the Institutional Animal Care and Use Committee of Thomas Jefferson University and Baylor College of Medicine.

METHOD DETAILS

Immunohistochemistry

Preparation of brains and brain sections from line J20 mice was performed as previously described (Corbett et al., 2017; You et al., 2017). Immunohistochemistry was performed on brain sections from line J20, as well as on brain sections from PSAPP mice and Tg2576 mice as previously described. PSAPP mice (Holcomb et al., 1998) express hAPP with the Swedish mutation and presenilin-1 with FAD mutation M146L, whereas Tg2576 mice (Hsiao et al., 1996) express human APP (hAPP) carrying the Swedish FAD mutation. Fixed brains were cryoprotected in 30% sucrose in phosphate-buffered saline, and coronal sections (30 μm) were cut on a sliding microtome (Microm). Sections were distributed into ten subseries, each containing every tenth section throughout the rostral-caudal extent of the brain. Each immunostain was performed on one full subseries of sections. For avidin-biotin/immunoperoxidase immunohistochemistry, sections were immunostained using mouse-anti-nestin (Millipore) or rabbit-anti-doublecortin (Cell Signaling) primary antibodies followed by biotinylated donkey anti-mouse or goat anti-rabbit secondary antibodies (Vector Laboratories). Diaminobenzidine was used as the chromagen. For immunofluorescence, goat anti-mouse secondary antibody (Jackson) was used. Immunoreactive neurons in the subgranular zone of the hippocampus were counted in every tenth coronal section throughout the rostral-caudal extent of the hippocampus and summed by an experimenter blinded to genotype and treatment. Neural stem cells, amplifying neural progenitors, neuroblasts, and immature neurons were identified by immunophenotyping on the basis of expression of nestin or doublecortin, and on morphology, following criteria previously published (Encinas and Enikolopov, 2008; Encinas et al., 2011b). For only the 1 month time point in Figures 1G, and 4C, DCX expression was assessed by taking the sum of the percent area of the subgranular zone and granule cell layer that was covered by a predesignated optical density threshold of DCX staining (modified from Jain et al., 2019). Data are shown normalized to control groups to illustrate genotype and/or treatment-specific differences; raw values are listed in Table S1. ΔFosB immunoreactivity quantification was performed by assessing the mean pixel intensity using ImageJ software. ΔFosB immunoreactivity was calculated as the ratio of the intensity of the granule cell layer and the stratum radiatum.

BrdU and EdU labeling

For neurogenesis time course experiments, BrdU (150 mg/kg, Sigma, St. Louis, MO) was dissolved in saline and administered twice intraperitoneally with injections spaced 2 hours apart. Mice were sacrificed 2 hours after the last BrdU injection. For levetiracetam treatment experiments, BrdU (100 mg/kg) was administered intraperitoneally on the final day of levetiracetam treatment. For kainic acid induction of neurogenesis experiments, BrdU (100 mg/kg) was administered intraperitoneally once per day for 7 days following treatment with kainic acid. Mice were sacrificed 24 hours after the last BrdU injection. Brain sections were stained with rat-anti-BrdU antibody (Accurate Chemical) followed by donkey-anti-rat secondary antibody conjugated to AlexaFluor-594 (Invitrogen). Prolong Gold antifade mounting medium with DAPI (Invitrogen) was used to allow visualization of nuclei. Labeling was visualized with epifluorescence microscopy. BrdU/nestin-positive cells in the subgranular zone of the hippocampus were counted in every tenth coronal section throughout the rostral-caudal extent of the hippocampus and summed by an experimenter blinded to genotype.

For double-labeling of BrdU and EdU, BrdU was first injected as described above (100mg/kg), and EdU (82mg/kg, Invitrogen) was dissolved in saline and administered intraperitoneally 22 hours later. Mice were sacrificed 2 hours after the EdU injection. BrdU and EdU were visualized with mouse anti-BrdU (Sigma), followed by goat anti-mouse Rhodamine (Jackson), and Click-iT EdU AlexaFluor 647 Imaging Kit (Invitrogen), respectively.

Neurosphere Experiments

Neurosphere experiments were performed as previously described (Bennett et al., 2009). APP mice were sacrificed at P3 or at P30 by decapitation. Both hippocampi from each mouse were dissected in cold PBS and incubated at 37°C for 10 minutes in 1ml enzyme (1mg/ml Papain, Roche and 1mg/ml DNase I, Roche). The hippocampi were then dissociated in fresh medium centrifuged at 200 g, at room temperature, for 5 minutes. The pellet was re-suspended into 2ml medium, filtered through a 70um cell strainer into 6-well ultra-low attachment plate. Cells were cultured in 3 mL complete medium containing 1xN2 (Life Technologies), 1xB27 (Life Technologies), 0.36U/ml Heparin (Sigma), 20ng/ml bFGF (R&D Systems) and 20ng/ml EGF (R&D Systems) at 37°C. The cell density was 2-6x10^5 per well. Cells were passaged every 5-6 days a total of four times before BrdU incorporation.

For BrdU incorporation, neurospheres were dissociated into single cells and plated into 24-well plate pre-coated with Geltrex (Life Technology) at 2-5x10^5 cells per well. The cells were kept in complete medium containing 2 uM BrdU (Sigma) for 24 hours. The cells were then fixed with 4% paraformaldehyde in PBS for 30min at 4°C and then treated with 2N HCl for 10 minutes at room temperature. They were then neutralized with sodium tetraborate and incubated with primary antibodies against BrdU (Accurate Chemical) and nestin (Millipore) overnight at 4°C. The cells were then incubated with Alexa Fluor 594-conjugated anti-rat IgG (Molecular Probe) and FITC-conjugated anti-mouse IgG (Jackson Immune) at room temperature, as well as with Hoechst 33342 to stain nuclei. Pictures were taken from five random fields per well. BrdU-positive cells and total cells were counted by an experimenter blinded to genotype.

EEG Recordings

Mice were stereotaxically implanted with a six-electrode array headcap for EEG monitoring. Teflon-coated silver wire (0.005 in diameter) attached to a 6-pin Delran pedestal (Plastics One) was wrapped around screws implanted bilaterally into the subdural space over frontal and temporal cortices (from Bregma:1.0 mm A-P, 1.5 mm M-L; −2.2 mm A-P, 2 mm M-L) along with a hippocampal depth electrode (−2.2 mm A-P, 2 mm M-L,1.8 mm from brain surface (DV)). All implants in 1 month old mice were depth electrodes. Ground and reference electrodes were implanted directly behind Lambda on either side of the midline. Mice were allowed to recover for at least 4 days before recordings were conducted. EEG recordings were performed in the home cage of the mice on at least two different days for a minimum of 8 hours per trial using a Stellate Harmonie acquisition system (version 7.0a, Natus Medical, Pleasonton, CA) with a sampling rate of 2000 Hz for data acquisition. Native Stellate and Lab Chart Pro (AD Instruments Inc.) software were used for EEG signal processing and spike count analyses.

Pharmacological Treatments

For assessment of the effect of levetiracetam on neurogenesis, levetiracetam (Sequoia Research Products, Pangbourne, United Kingdom) was dissolved in saline and injected intraperitoneally at a dose of 75 mg/kg, 3 times per day for 2 weeks. Control groups were administered with the equivalent volume of saline. Two APP mice that received levetiracetam treatment were observed still having seizures, and were excluded from analysis. For assessment of the effect of levetiracetam on spatial discrimination behavior, levetiracetam was delivered via Alzet micro-osmotic pumps (model 1004) at a dose of 75 mg/kg/day. Micro-osmotic pumps were filled with saline or levetiracetam per manufacturer's instructions, and primed for 2 days prior to implantation subcutaneously into the intrascapular region. Model 1004 micro-osmotic pumps delivered fluid at a rate of 0.11 μL/hr for 28 days.

For kainic acid seizures, kainic acid (Sigma) was dissolved in saline and injected intraperitoneally at a dose of 15 mg/kg. Control groups were administered with the equivalent volume of saline. Seizures were behaviorally monitored and scored for the first two hours post injection.

Spatial Discrimination Task

The experimental design was based on previously published protocols (Wimmer et al., 2012; You et al., 2017). The experimental apparatus consisted of an empty mouse housing cage placed within a three-sided white enclosure, directly touching one side. To provide visual cues for spatial orientation, the back wall of the enclosure was striped with black tape, the side wall adjacent to the cage had an A4-sized picture taped to it, and a small box was placed to the left of the mouse cage. Two 25 mL Erlenmeyer flasks were placed equidistant to the two corners of the cage facing the striped wall (see Figure 5A). For the training phase, mice were individually placed in the center of the cage and allowed to freely explore for three, 3-minute training sessions separated by 3-minute rest periods in their home cages. For the test trial, which took place 3 minutes after the last training trial, one of the two flasks was displaced to varying distances (one, two, three, or four flask lengths) from its original location before the mice were placed back in the cage for the single 3-minute testing session. During each trial, the amount of time spent exploring each of the two Erlenmeyer flasks was measured by an experimenter blinded to genotype/treatment.

QUANTIFICATION AND STATISTICAL ANALYSIS

Bias Elimination and Randomization

No specific method of randomization of mice was used, but mice were semirandomly assigned to experimental groups on the basis of birth order after balancing for age, sex, and genotype. Experiments were performed and quantified by investigators who were blinded to the genotype and treatment of the mice, and were unblinded once summary data was ready to be prepared.

Statistical Analysis

GraphPad Prism 6.0 was used for statistical analyses. For comparisons between two experimental groups, unpaired two-tailed Student t tests were used. With respect to neurogenesis or neural stem cell markers, t tests were used to compare NTG and APP mice at each age, as the experiments were designed and powered to assess the difference between genotypes at each individual age. One-tailed unpaired Student t tests were used when there were *a priori* assumptions made about direction of change (Figure S3). For comparisons between more than two experimental groups, a two-way ANOVA test (when there was normal sample distribution) or a Kruskal–Wallis test (when normality could not be assumed) was used. When two-way ANOVA and Kruskal-Wallis tests were statistically significant, multiple-comparison post hoc analyses were performed to compare the differences between individual groups. A p value of less than 0.05 was considered statistically significant. The statistical tests, n (number of animals), and p values for each dataset are provided in the figure legend that accompanies the data. Detailed results of all statistical analyses are listed in Table S2.

Cell Reports, Volume *27*

Supplemental Information

Early Seizure Activity Accelerates Depletion of Hippocampal Neural Stem Cells and Impairs Spatial Discrimination in an Alzheimer's Disease Model

Chia-Hsuan Fu, Daniel Maxim Iascone, Iraklis Petrof, Anupam Hazra, Xiaohong Zhang, Mark S. Pyfer, Umberto Tosi, Brian F. Corbett, Jingli Cai, Jason Lee, Jin Park, Lorraine Iacovitti, Helen E. Scharfman, Grigori Enikolopov, and Jeannie Chin

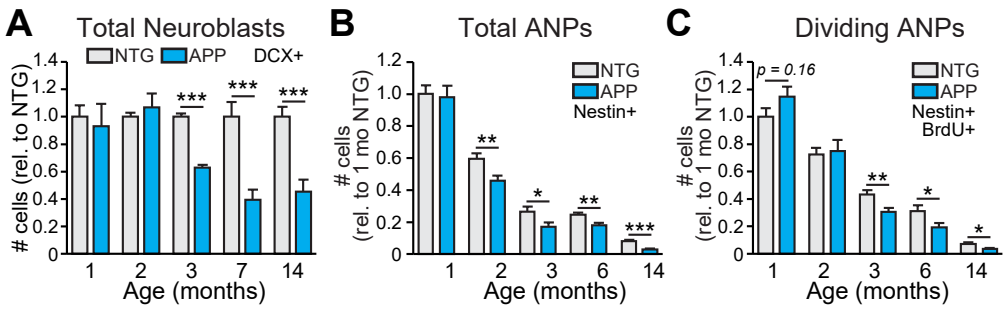

Figure S1. The effects of seizures on neuroblasts and amplifying neural progenitors (ANPs). Related to Figures 1 and 2.
(A) Optical density measurement of DCX at 1 month of age (n = 9-12 mice per genotype), and number of DCX+ neuroblasts at 2 (n = 6 mice per genotype), 3 (n = 8 mice per genotype), 7 (n = 9-10 mice per genotype), and 14 (n = 11-12 mice per genotype) months of age, normalized to NTG at each time point. Note that the 1 month time point is the same data as presented in Fig 1D.
(B) Numbers of Nestin+ ANPs were quantified in NTG and APP at 1 (n = 10-11 mice per genotype), 2 (n = 14 mice per genotype), 3 (n = 8 mice per genotype), 6 (n = 9-10 mice per genotype), and 14 (n = 11-12 mice per genotype) months of age. Cell counts are presented here as normalized to the average of 1-month-old NTG mice.
(C) Number of BrdU+ Nestin+ ANPs were quantified in NTG and APP mice at 1 (n = 9-10 mice per genotype), 2 (n = 8 mice per genotype), 3 (n = 8 mice per genotype), 6 (n = 8 mice per genotype), and 14 (n = 11-12 mice per genotype) months of age. Cell counts are presented here as normalized to the average of 1-month-old NTG mice.
*$p < 0.05$; **$p < 0.01$, ***$p < 0.001$, two-tailed unpaired Student's t-test comparing means between NTG and APP mice at each age (A-C).

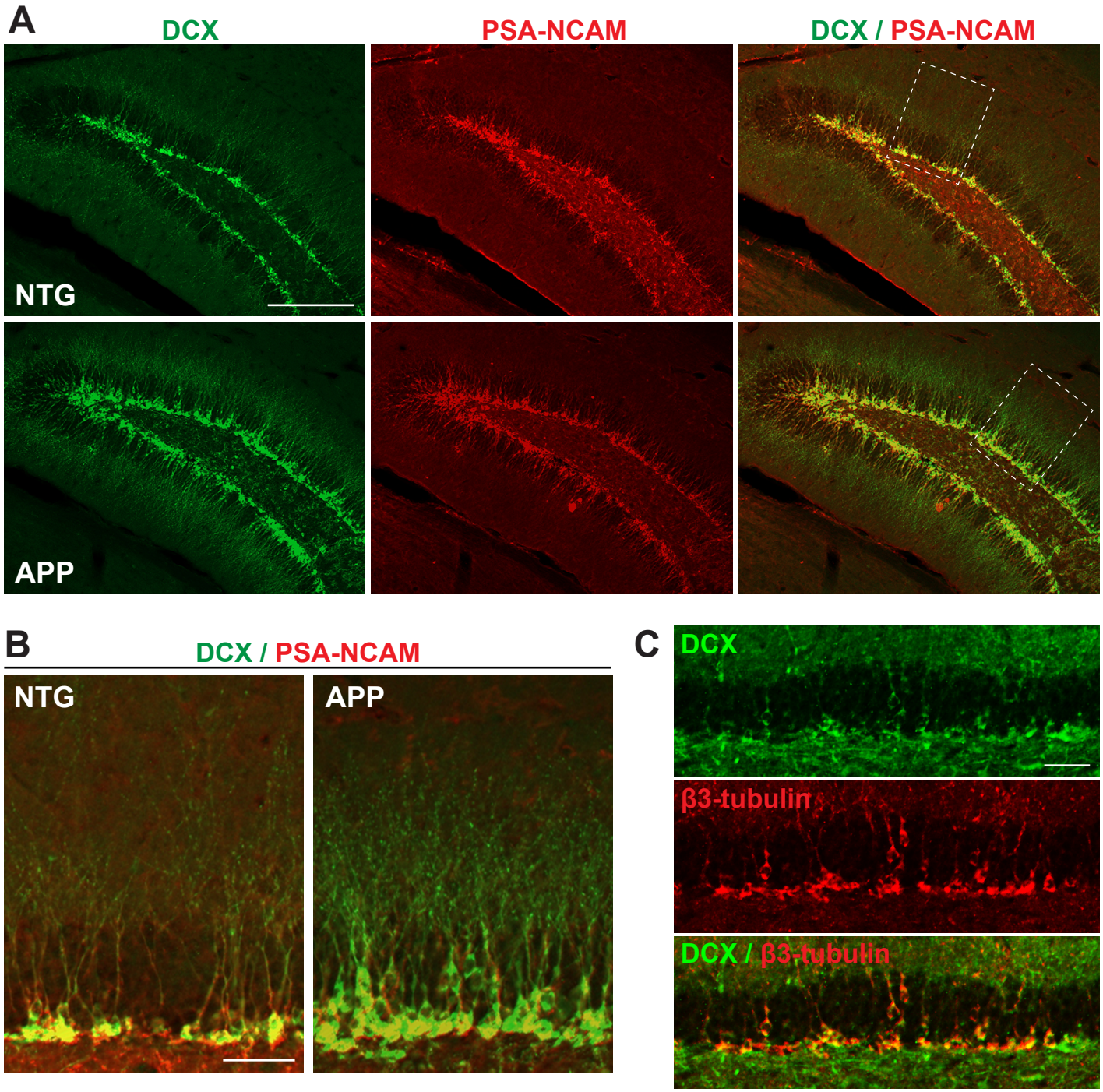

Figure S2. Doublecortin-expressing cells in the dentate gyrus of NTG and APP mice also express PSA-NCAM and β3-tubulin. Related to Figure 1.

Coronal sections from mice at 2 months of age were immunostained.

(A) Doublecortin (green, left panels) is expressed in cell bodies and in dendritic processes, as is PSA-NCAM (red, middle panels). Overlaid images (right panels) reveal coexpression of doublecortin and PSA-NCAM (yellow) in neurons in the subgranular zone of NTG mice (top panels) and APP mice (bottom panels). Scale bar, 200μm.

(B) Inset of are indicated in overlaid images in A. Note that the increase in doublecortin- and PSA-NCAM-expressing neurons is evident at this age, consistent with findings in Figure 1 of the main paper. Scale bar, 50μm.

(C) Doublecortin-expressing cells (green, top panel) also express β3-tubulin, a marker of neuronal cells (red, middle panel; see overlay, bottom panel). Scale bar, 50μm.

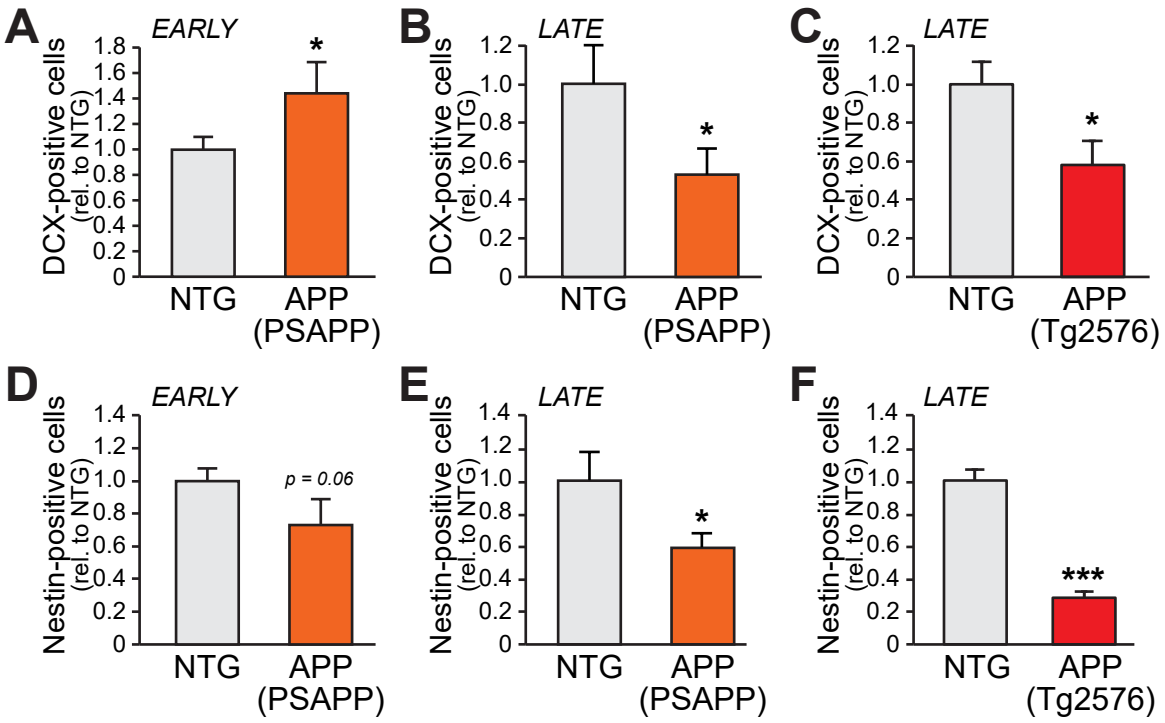

Figure S3. The PSAPP and TG2576 lines of transgenic APP mice exhibit alterations in immature neurons and neural stem cells similar to J20 APP mice. Related to Figures 1 and 2.

Brain sections from PSAPP mice at 5 months of age (n = 9-11 mice per genotype) and 12 months of age (n = 11-12 mice per genotype), and from Tg2576 mice at 10 months of age (n = 11 mice per genotype) were immunostained for doublecortin and nestin.

(A-B) Immunostaining of brain sections from PSAPP mice demonstrate increased number of DCX-expressing immature neurons at early disease stages (5 months of age, A) and decreased numbers at late disease stages (12 months of age, B) compared with age-matched controls.

(C) Tg2576 mice at late disease stages (10 months of age) also showed decreased DCX-expressing newborn neurons.

(D-E) PSAPP mice exhibit modest decreases in nestin-expressing neural stem cells at early disease stages (D) that further decrease at later disease stages (E).

(F) Tg2576 mice at late disease stages also show decreased Nestin-expressing neural stem cells compared with NTG controls.

For statistical analyses, one-tailed unpaired Student's t-tests were used since the hypothesis was that the direction of change in PSAPP and Tg2576 mice would mirror that observed in J20 mice in Figures 1 and 2, *$p < 0.01$, *** $p < 0.001$. Values indicate mean ± SEM.

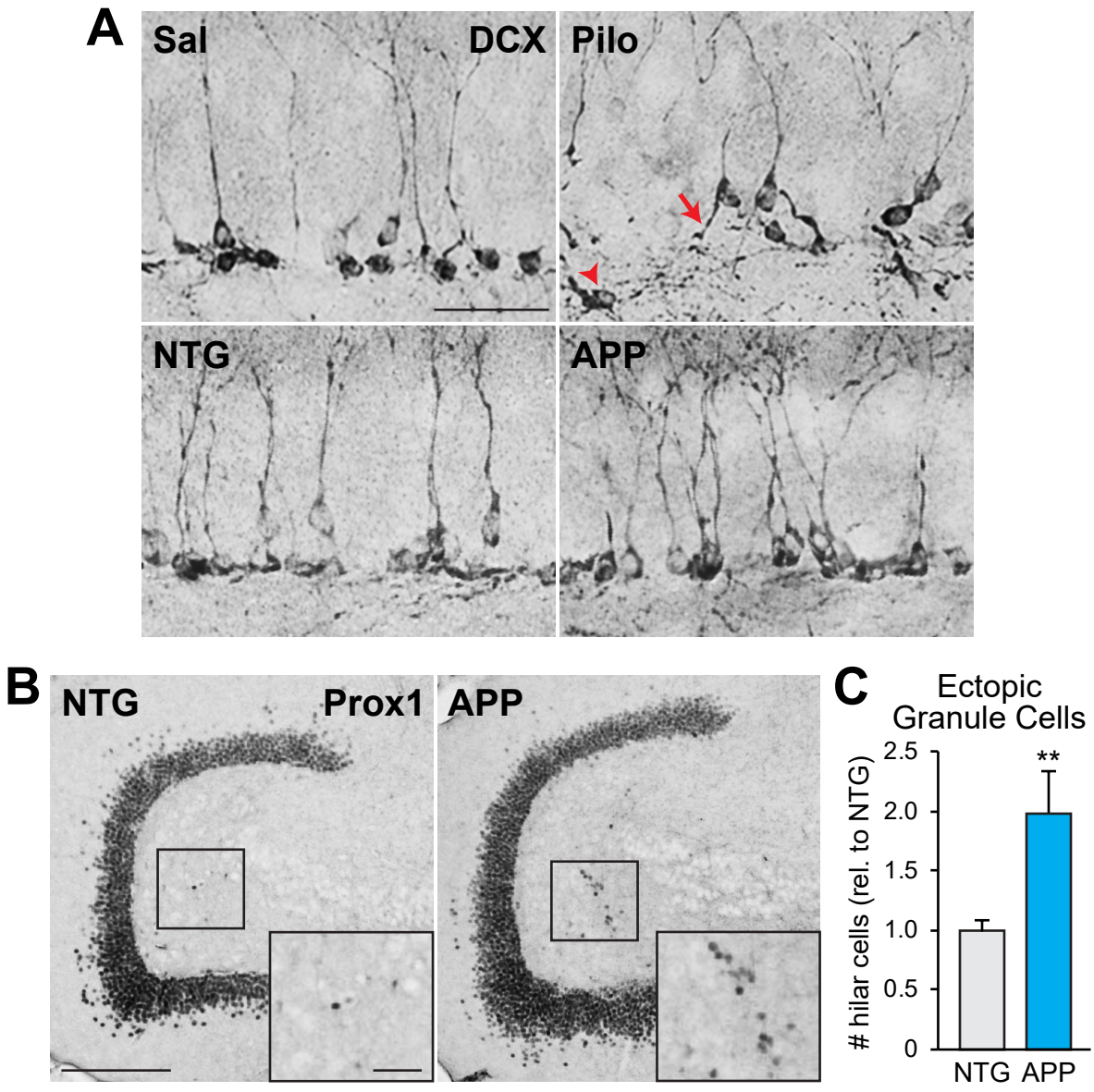

Figure S4. Newborn neurons in APP mice exhibit normal morphology, but show increased ectopic migration into the hilus compared to NTG mice. Related to Figure 1.

(A) Morphology of DCX+ cells is not obviously different between NTG and APP mice (3 months of age). In contrast, pilocarpine-treated wild-type mice (270-280 mg/kg, IP, 6 weeks post status epilepticus) showed altered neuronal polarity (arrow) and migration (arrowhead) compared to saline-treated mice. Scale bar, 50µm.

(B) APP mice show increased number of ectopic Prox1+ granule neurons in the hilus compared to NTG mice (6 months of age, n = 7-10 mice per genotype). Scale bar, 250µm, inset scale bar, 50µm.

**$p < 0.01$, two-tailed unpaired Student's t-test. Values indicate mean ± SEM.

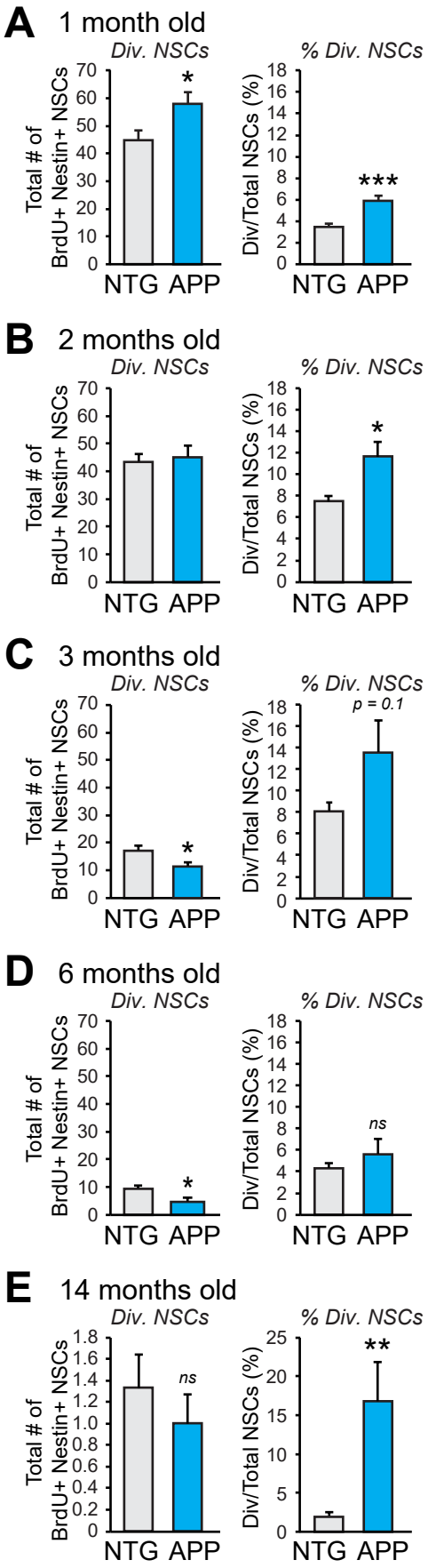

Figure S5. APP mice exhibit altered NSC division at different ages. Related to Figure 2.

(A-E) Neural stem cell (NSC) division is represented as total number of BrdU+ Nestin+ dividing NSCs (left), and as a percentage of dividing NSCs/total NSCs (right) in NTG and APP mice at 1 (A, n = 9-10 mice per genotype), 2 (B, n = 8 mice per genotype), 3 (C, n = 8 mice per genotype), 6 (D, n = 8 mice per genotype), and 14 (E, n = 11-12 mice per genotype) months of age.

*p < 0.05; **p < 0.01, ***p < 0.001, *ns*, not significant, two-tailed unpaired Student's t-test. Values indicate mean ± SEM.

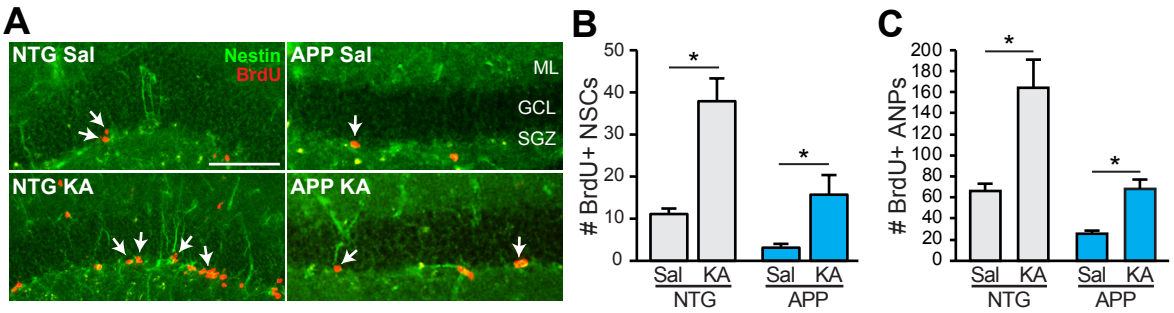

Figure S6. Kainic acid seizures induce NSC division in NTG and APP mice. Related to Figures 2 and 3.
(A) Representative images of Nestin/BrdU staining in 8-month-old NTG and APP mice that received intraperitoneal injection of saline or kainic acid (KA, 15 mg/kg). Scale bar, 100μm.
(B) Number of BrdU+ Nestin+ NSCs in the SGZ of NTG and APP mice injected with saline or kainic acid (n = 7-13 mice per genotype and treatment). Kruskal-Wallis test revealed significant differences between groups ($p < 0.0001$).
(C) Number of BrdU+ Nestin+ ANPs in the SGZ of NTG and APP mice injected with either saline or kainic acid (n = 7-13 mice per genotype and treatment). Kruskal-Wallis test revealed significant differences between groups ($p < 0.0001$).
*$p < 0.05$, Dunn post-hoc test. Values indicate mean ± SEM.

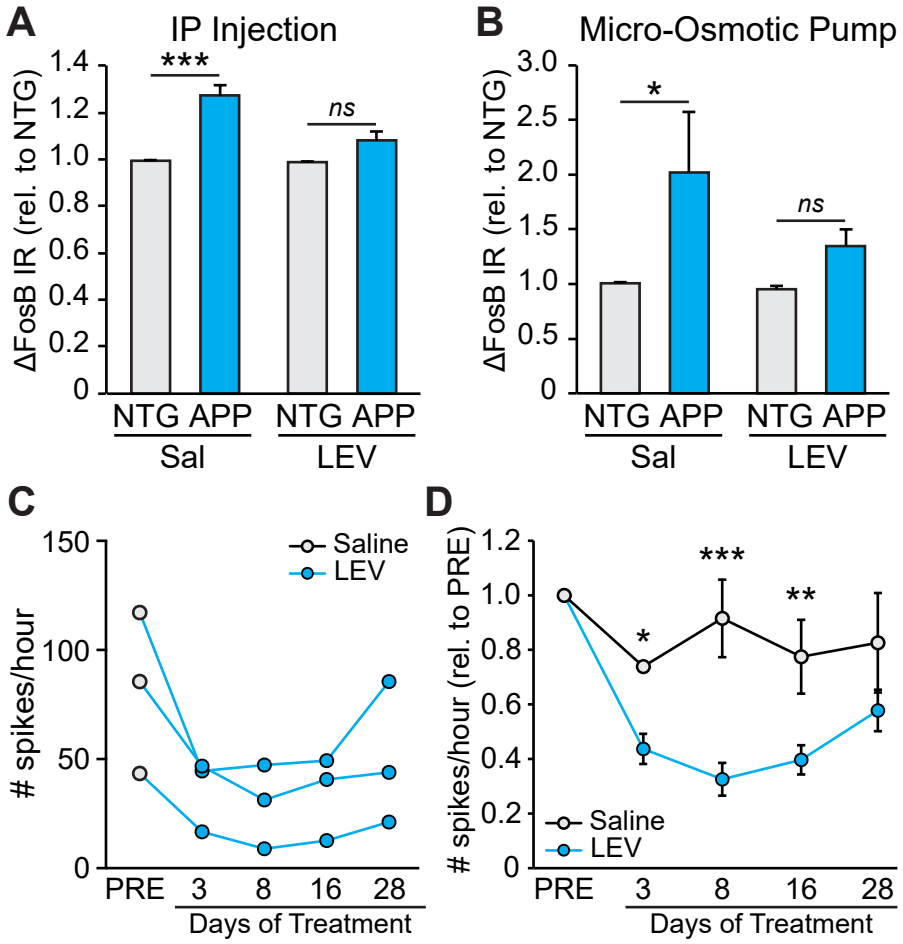

Figure S7. Treatment of APP mice with the antiepileptic drug levetiracetam normalizes ΔFosB, a seizure-induced transcription factor, and epileptic spikes. Related to Figures 4 and 5.

(A) Mice in Figure 6 were injected with levetiracetam (LEV, 75 mg/kg, IP), or an equivalent volume of saline, 3 times a day for 2 weeks (n = 9-11 mice per genotype/treatment), and then sacrificed and brains were processed for immunostaining. Δ FosB immunoreactivity (IR) is increased in saline-treated APP mice compared with saline-treated NTG mice, but is normalized in LEV-treated APP mice compared to LEV-treated NTG mice. Two-way ANOVA revealed a significant effect of LEV treatment ($p < 0.01$), genotype ($p < 0.0001$), and an interaction between treatment and genotype ($p < 0.01$).

(B) Mice in Figure 7 were implanted with Alzet micro-osmotic pumps designed to release either saline or 75 mg/kg/day of LEV for 28 days (n = 6-8 mice per genotype/treatment). LEV delivered via micro-osmotic pumps similarly reduced ΔFosB IR in APP mice. Two-way ANOVA revealed a significant effect of genotype ($p < 0.05$).

*$p < 0.05$, ****$p < 0.0001$, *ns*, not significant, Tukey post-hoc tests (A-B).

(C-D) Mice received implantation of chronic EEG electrodes, allowed to recover, and baseline EEG recordings were performed. Mice were then implanted with Alzet micro-osmotic pumps designed to release 75 mg/kg/day of LEV for 28 days.

(C) Number of spikes exhibited by individual mice during baseline recordings, and then at 3, 8, 16, and 28 days of LEV treatment.

(D) Data in panel C was normalized to baseline spike frequency (blue circles), and plotted with data from mice that received saline-filled micro-osmotic pumps as controls (gray circles). Two-way repeated measures ANOVA revealed a significant effect of LEV treatment ($p < 0.05$), and an interaction between treatment and time ($p < 0.01$).

Holm-Sidak post-hoc tests indicated significant differences between saline and LEV groups at 3, 8, and 16 days of treatment.

*$p < 0.05$, **$p < 0.01$, ***$p < 0.001$, *ns*, not significant. Values indicate mean ± SEM.

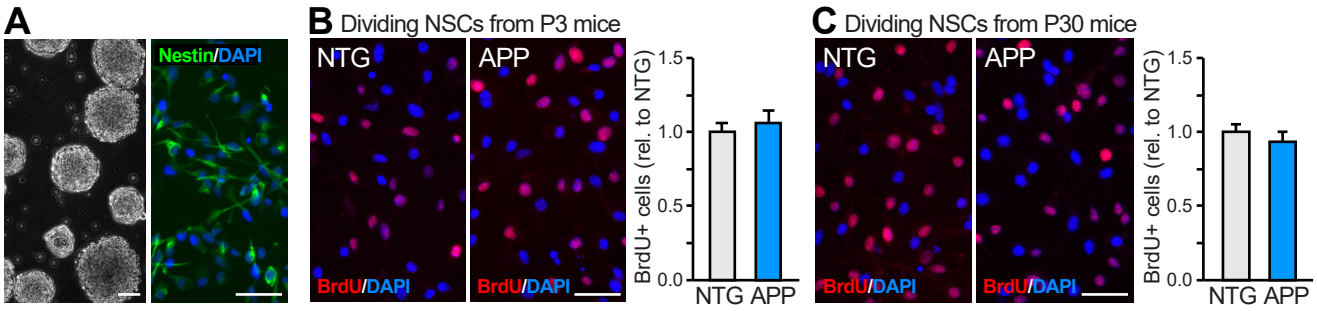

Figure S8. NSCs division is similar in dissociated neurospheres from NTG and APP mice. Related to Figure 4.
(A) Representative images of neurospheres grown in vitro from hippocampal NSCs (left) that can be dissociated, plated, and immunostained for nestin and DAPI to confirm their identity (right).
(B) Example images of BrdU+ NSCs generated from dissociated neurospheres originating from mice at postnatal day 3 (P3, left), with quantification (right; n = 3 mice per genotype).
(C) Example images of BrdU+ dividing NSCs generated from dissociated neurospheres originating from mice at postnatal day 30 (P30, left), with quantification (right; n = 4 mice per genotype).
Scale bars: (A) left, 100µm; right, 50µm. (B, C) 50µm. Two-tailed unpaired Student's t test. Values indicate mean ± SEM.

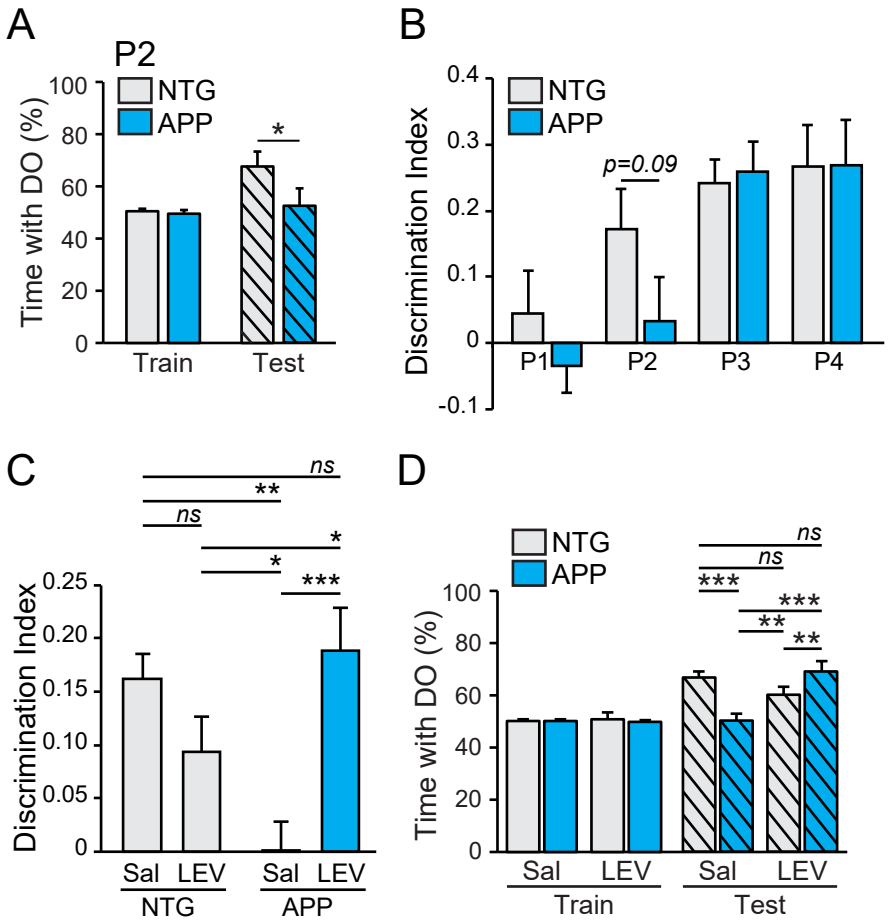

Figure S9. Spatial discrimination index of NTG and APP mice. Related to Figure 5.
(A-B) Additional analyses of data presented in Figure 5B.
(A) Comparison of spatial discrimination performance at position 2 in untreated NTG and APP mice. Two-way ANOVA revealed a significant effect of test phase ($p < 0.05$). *$p < 0.05$, Holm-Sidak post-hoc test. For simplicity, post-hoc comparisons for only the "Test" phase are indicated.
(B) Discrimination index was calculated as the difference between the percent of time spent with displaced object during the testing and training phases of the spatial discrimination task in untreated NTG and APP mice. Two-way ANOVA revealed a significant effect of object position ($p < 0.0001$). $p = 0.09$, Fisher's LSD post-hoc test.
(C-D) Additional analyses of data presented in Figure 5C.
(C) Discrimination index at position 2 in saline- or LEV-treated NTG and APP mice. Two-way ANOVA revealed a significant effect of LEV treatment ($p < 0.05$) and an interaction between genotype and treatment ($p < 0.001$). *$p < 0.05$, **$p < 0.01$, ***$p < 0.001$, ns, not significant, Newman-Keuls post-hoc test.
(D) Comparison of spatial discrimination performance at position 2 in saline- or LEV-treated NTG and APP mice. Two-way ANOVA revealed a significant effect of LEV treatment ($p < 0.001$), test phase ($p < 0.0001$), and an interaction between treatment and test phase ($p < 0.001$). **$p < 0.01$, ***$p < 0.001$, *ns*, not significant, Holm-Sidak post-hoc test. For simplicity, post-hoc comparisons for only the "Test" phase are indicated. Values indicate mean ± SEM.

Table S1. Raw values for normalized data in Figures 1-S8. Related to Figures 1-S8 and STAR Methods

Figure	Parameter	Groups	Avg ± SEM	Additional cohort	Unit
1g	DCX+ staining	NTG (1 mo) APP (1 mo)	148.39 ± 12.24 137.93 ± 24.23		Sum of % threshold area covered by DCX expression in the granule cell layer in every 10th section through the rostral-caudal extent of hippocampus.
	DCX+ immature neurons	NTG (2 mo) APP (2 mo) NTG (3 mo) APP (3 mo) NTG (7 mo) APP (7 mo) NTG (14 mo) APP (14 mo)	665.83 ± 45.79 903.50 ± 95.33 515.63 ± 17.18 394.63 ± 39.91 167.40 ± 14.57 54.67 ± 15.06 50.58 ± 3.19 19.36 ± 7.33		Cell numbers
2c	Nestin+ NSCs	NTG (1 mo) APP (1 mo) NTG (2 mo) APP (2 mo) NTG (3 mo) APP (3 mo) NTG (6 mo) APP (6 mo) NTG (14 mo) APP (14 mo)	977.36 ± 38.86 910.67 ± 52.63 373.00 ± 28.36 144.83 ± 23.20 217.50 ± 9.65 124.63 ± 28.97 172.40 ± 13.72 85.22 ± 15.12 72.83 ± 3.91 9.45 ± 4.39	 592.50 ± 49.18 411.88 ±49.26	Cell numbers
2f	Nestin+ BrdU+ NSCs	NTG (1 mo) APP (1 mo) NTG (2 mo) APP (2 mo) NTG (3 mo) APP (3 mo) NTG (6 mo) APP (6 mo) NTG (14 mo) APP (14 mo)	45.11 ± 3.32 58.10 ± 4.30 43.63 ± 2.76 45.25 ± 4.17 17.38 ± 1.59 11.50 ± 1.55 9.57 ± 1.13 4.88 ± 1.33 1.33 ± 0.31 1.00 ± 0.27		Cell numbers
2i	Nestin+ Ki67+ NSCs	NTG APP	50.25 ± 4.26 57.13 ± 7.21		Cell numbers
3b, c	BrdU+ EdU+ Nestin+ NSCs	NTG (3 wk) APP (3 wk) NTG (2 mo) APP (2 mo) NTG (6 mo) APP (6 mo) NTG (12 mo) APP (12 mo)	39.83 ± 5.21 76.67 ± 13.70 18.25 ± 2.10 13.33 ± 2.82 3.43 ± 0.84 1.25 ± 0.49 3.33 ± 0.67 0.40 ± 0.24		Cell numbers
4a	Ki67+ Nestin+ NSCs/ Nestin+ NSCs	NTG sal APP sal NTG lev APP lev	18.53 ± 2.15 30.68 ± 5.97 17.96 ± 2.04 26.04 ± 3.91	7.75 ± 1.25 18.22 ± 4.09 5.06 ± 1.25 7.83 ± 3.10	% Cell numbers
4b	Nestin+ NSCs	NTG sal APP sal NTG lev APP lev	484.50 ± 60.04 225.75 ± 45.75 494.60 ± 55.44 365.00 ± 57.04	186.2 ± 17.93 134 ± 18.87 173.33 ± 7.80 184.80 ± 25.70	Cell numbers
4c	DCX+ staining	NTG sal APP sal NTG lev APP lev	198.73 ± 7.23 259.61 ± 25.71 157.16 ± 22.38 132.59 ± 46.75	110.03 ± 8.28 181.82 ± 32.31 83.13 ± 4.31 116.29 ± 24.65	Sum of % threshold area covered by DCX expression in the granule cell layer in every 10th section through the rostral-caudal extent of hippocampus.
S1a	DCX+ staining	NTG (1 mo) APP (1 mo)	148.39 ± 12.24 137.93 ± 24.23		Sum of % threshold area covered by DCX expression in the granule

					cell layer in every 10th section through the rostral-caudal extent of hippocampus.
	DCX+ neuroblasts	NTG (2 mo) APP (2 mo) NTG (3 mo) APP (3 mo) NTG (7 mo) APP (7 mo) NTG (14 mo) APP (14 mo)	992.50 ± 28.05 1058 ± 102.75 640.38 ± 14.36 402.25 ± 11.91 506.90 ± 53.50 199.56 ± 37.43 56.58 ± 4.00 25.55 ± 4.99		Cell numbers
S1b	Nestin+ ANPs	NTG (1 mo) APP (1 mo) NTG (2 mo) APP (2 mo) NTG (3 mo) APP (3 mo) NTG (6 mo) APP (6 mo) NTG (14 mo) APP (14 mo)	853.36 ± 43.08 836.44 ± 57.67 567.00 ± 38.86 427.17 ± 21.51 225.75 ± 27.21 145.5 ± 22.09 208.40 ± 12.05 152.89 ± 12.17 68.67 ± 6.12 23.64 ± 4.68	 463.63 ± 34.93 361.75 ± 44.07	Cell numbers
S1c	Nestin+ BrdU+ ANPs	NTG (1 mo) APP (1 mo) NTG (2 mo) APP (2 mo) NTG (3 mo) APP (3 mo) NTG (6 mo) APP (6 mo) NTG (14 mo) APP (14 mo)	137.67 ± 8.42 157.5 ± 10.29 99.50 ± 6.58 103 ± 11.31 59.50 ± 4.19 42.00 ± 4.09 42.71 ± 5.69 26.25 ± 4.58 9.58 ± 1.78 4.64 ± 1.08		Cell numbers
S3a	DCX+ immature neurons	NTG PSAPP	163.91 ± 15.82 241.89 ± 40.51		Cell numbers
S3b	DCX+ immature neurons	NTG PSAPP	32.45 ± 6.56 16.33 ± 4.13		Cell numbers
S3c	DCX+ immature neurons	NTG Tg2576	53.09 ± 6.14 30.80 ± 6.82		Cell numbers
S3d	Nestin+ NSCs	NTG PSAPP	159.09 ± 11.83 116.22 ± 25.10		Cell numbers
S3e	Nestin+ NSCs	NTG PSAPP	71 ± 12.06 41.75 ± 6.10		Cell numbers
S3f	Nestin+ NSCs	NTG Tg2576	103.50 ± 6.95 29.78 ± 3.79		Cell numbers
S4c	Prox1+ hilar granule cells	NTG APP	83.50 ± 7.22 165.86 ± 29.57		Cell numbers
S7a	ΔFosB IR	NTG sal APP sal NTG LEV APP LEV	1.109 ± 0.007 1.426 ± 0.088 1.102 ± 0.004 1.240 ± 0.059	1.075 ± 0.004 1.366 ± 0.066 1.072 ± 0.003 1.102 ± 0.020	Arbitrary units (intensity)
S7b	ΔFosB IR	NTG sal APP sal NTG LEV APP LEV	1.682 ± 0.022 4.881 ± 1.448 1.434 ± 0.045 2.860 ± 0.549	1.047 ± 0.003 1.186 ± 0.107 1.051 ± 0.005 1.187 ± 0.061	Arbitrary units (intensity)
S8b	BrdU+ cells	NTG APP	41.60 ± 2.45 44.12 ± 3.66		Cell numbers
S8c	BrdU+ cells	NTG APP	52.94 ± 2.84 49.34 ± 3.66		Cell numbers

Table S2. Statistical values for comparisons in Figures 1-S9. Related to Figures 1-S9 and STAR Methods.

Figure	Parameter	Groups	Test used	Values	P value
1d	Spikes per hour	NTG, APP (1 mo) NTG, APP (2 mo) NTG, APP (4-6 mo)	Student t-test, 2-tailed	$t_6 = 2.514$ $t_4 = 4.209$ $t_6 = 3.879$	P = 0.0456 P = 0.0136 P = 0.0082
1g	DCX+ staining	NTG, APP (1 mo)	Student t-test, 2-tailed	$t_{19} = 0.4153$	P = 0.6826
	DCX+ immature neurons	NTG, APP (2 mo) NTG, APP (3 mo) NTG, APP (7 mo) NTG, APP (14 mo)	Student t-test, 2-tailed	$t_{10} = 2.247$ $t_{14} = 2.785$ $t_{17} = 5.374$ $t_{21} = 4.024$	P = 0.0484 P = 0.0146 P < 0.0001 P = 0.0006
2c	Nestin+ NSCs	NTG, APP (1 mo) NTG, APP (2 mo) NTG, APP (3 mo) NTG, APP (7 mo) NTG, APP (14 mo)	Student t-test, 2-tailed	$t_{18} = 1.011$ $t_{26} = 5.002$ $t_{14} = 3.041$ $t_{17} = 3.399$ $t_{21} = 10.81$	P = 0.3254 P < 0.0001 P = 0.0088 P = 0.0034 P < 0.0001
2f	Nestin+ BrdU+ NSCs	NTG, APP (1 mo) NTG, APP (2 mo) NTG, APP (3 mo) NTG, APP (7 mo) NTG, APP (14 mo)	Student t-test, 2-tailed	$t_{17} = 2.353$ $t_{14} = 0.3248$ $t_{14} = 2.647$ $t_{13} = 2.649$ $t_{21} = 0.8050$	P = 0.0309 P = 0.7501 P = 0.0191 P = 0.0201 P = 0.4299
	BrdU+ Nestin+ NSCs/ Nestin+ NSCs	NTG, APP (2 mo, inset)	Student t-test, 2-tailed	$t_{14} = 2.925$	P = 0.0111
2i	Nestin+ Ki67+ NSCs	NTG, APP	Student t-test, 2-tailed	$t_{14} = 0.8213$	P = 0.4253
	Ki67+ Nestin+ NSCs/ Nestin+ NSCs	NTG, APP	Student t-test, 2-tailed	$t_{14} = 2.141$	P = 0.0504
3b, c	BrdU+ EdU+ Nestin+ NSCs	NTG, APP (3 wk) NTG, APP (2 mo) NTG, APP (6 mo) NTG, APP (12 mo)	Student t-test, 2-tailed	$t_{10} = 2.514$ $t_{12} = 1.429$ $t_{13} = 2.309$ $t_{12} = 3.162$	P = 0.0307 P = 0.1784 P = 0.0380 P = 0.0082
4a	Ki67+ Nestin+ NSCs/ Nestin+ NSCs	NTG, APP (saline) NTG, APP (LEV)	2-way ANOVA	Genotype, $F_{1,35} = 8.785$ Treatment, $F_{1,35} = 6.929$ Interaction, $F_{1,35} = 3.095$	P = 0.0054 P = 0.0125 P = 0.0873
		NTG sal v NTG LEV NTG sal v APP sal NTG sal v APP LEV NTG LEV v APP sal NTG LEV v APP LEV APP sal v APP LEV	Holm-Sidak post-hoc	$t_{35} = 0.6278$ $t_{35} = 3.397$ $t_{35} = 0.2205$ $t_{35} = 4.242$ $t_{35} = 0.8379$ $t_{35} = 3.055$	P = 0.7923 P = 0.0085 P = 0.8267 P = 0.0009 P = 0.7923 P = 0.0170
4b	Nestin+ NSCs	NTG, APP (saline) NTG, APP (LEV)	2-way ANOVA	Genotype, $F_{1,35} = 7.003$ Treatment, $F_{1,35} = 2.925$ Interaction, $F_{1,35} = 4.273$	P = 0.0121 P = 0.0961 P = 0.0462
		NTG sal v NTG LEV NTG sal v APP sal NTG sal v APP LEV NTG LEV v APP sal NTG LEV v APP LEV APP sal v APP LEV	Holm-Sidak post-hoc	$t_{35} = 0.2567$ $t_{35} = 3.390$ $t_{35} = 0.6227$ $t_{35} = 3.303$ $t_{35} = 0.4029$ $t_{35} = 2.628$	P = 0.9036 P = 0.0104 P = 0.9011 P = 0.0110 P = 0.9036 P = 0.0497
4c	DCX+ staining	NTG, APP (saline) NTG, APP (LEV)	2-way ANOVA	Genotype, $F_{1,35} = 2.658$ Treatment, $F_{1,35} = 19.77$ Interaction, $F_{1,35} = 6.738$	P = 0.1120 P < 0.0001 P = 0.0137
		NTG sal v NTG LEV NTG sal v APP sal NTG sal v APP LEV NTG LEV v APP sal NTG LEV v APP LEV APP sal v APP LEV	Holm-Sidak post-hoc	$t_{35} = 1.331$ $t_{35} = 3.039$ $t_{35} = 1.873$ $t_{35} = 4.606$ $t_{35} = 0.6716$ $t_{35} = 4.899$	P = 0.3470 P = 0.0177 P = 0.1942 P = 0.0003 P = 0.5063 P = 0.0001
5b	Time spent with DO	NTG (P1, P2, P3, P4)	2-way RM ANOVA	Position, $F_{3,26} = 0.7074$ Test phase, $F_{1,26} = 38.39$ Interaction, $F_{3,26} = 2.992$	P=0.5563 P<0.0001 P=0.0492
		NTG P1 train v test	Holm-Sidak post-hoc	$t_{26} = 0.7706$	P = 0.4479

		NTG P2 train v test NTG P3 train v test NTG P4 train v test		t_{26} = 3.049 t_{26} = 3.990 t_{26} = 4.436	P = 0.0104 P = 0.0014 P = 0.0006
		APP (P1, P2, P3, P4)	2-way RM ANOVA	Position, $F_{3,23}$ = 7.271 Test phase, $F_{1,23}$ = 21.95 Interaction, $F_{3,23}$ = 7.783	P = 0.0013 P = 0.0001 P = 0.0009
		APP P1 train v test APP P2 train v test APP P3 train v test APP P4 train v test	Holm-Sidak post-hoc	t_{23} = 0.6623 t_{23} = 00.5999 t_{23} = 04.730 t_{23} = 04.533	P = 0.7641 P = 0.7641 P = 0.0004 P = 0.0004
5c	Time spent with DO	NTG, APP (saline) NTG, APP (LEV)	2-way RM ANOVA	Treatment, $F_{3,26}$ = 8.161 Test phase, $F_{1,26}$ = 59.59 Interaction, $F_{3,26}$ = 8.261	P = 0.0005 P < 0.0001 P = 0.0005
		NTG sal train v test NTG LEV train v test APP sal train v test APP LEV train v test	Holm-Sidak post-hoc	t_{26} = 5.593 t_{26} = 3.250 t_{26} = 0.02989 t_{26} = 7.192	P < 0.0001 P = 0.0064 P = 0.9764 P < 0.0001
S1a	DCX+ staining	NTG, APP (1 mo)	Student t-test, 2-tailed	t_{19} = 0.4153	P = 0.6826
	DCX+ neuroblasts	NTG, APP (2 mo) NTG, APP (3 mo) NTG, APP (7 mo) NTG, APP (14 mo)	Student t-test, 2-tailed	t_{10} = 0.6150 t_{14} = 12.76 t_{17} = 4.606 t_{21} = 4.892	P = 0.5523 P < 0.0001 P = 0.0003 P < 0.0001
S1b	Nestin+ ANPs	NTG, APP (1 mo) NTG, APP (2 mo) NTG, APP (3 mo) NTG, APP (7 mo) NTG, APP (14 mo)	Student t-test, 2-tailed	t_{18} = 0.2284 t_{26} = 3.104 t_{14} = 2.290 t_{17} = 3.233 t_{21} = 5.764	P = 0.8219 P = 0.0046 P = 0.0381 P = 0.0049 P < 0.0001
S1c	Nestin+ BrdU+ ANPs	NTG, APP (1 mo) NTG, APP (2 mo) NTG, APP (3 mo) NTG, APP (7 mo) NTG, APP (14 mo)	Student t-test, 2-tailed	t_{17} = 1.471 t_{14} = 0.2674 t_{14} = 2.987 t_{13} = 2.278 t_{21} = 2.321	P = 0.1596 P = 0.7931 P = 0.0098 P = 0.0403 P = 0.0304
S3a	DCX+ immature neurons	NTG, PSAPP	Student t-test, 1-tailed	t_{18} = 2.022	P = 0.0292
S3b	DCX+ immature neurons	NTG, PSAPP	Student t-test, 1-tailed	t_{20} = 1.921	P = 0.0346
S3c	DCX+ immature neurons	NTG, Tg2576	Student t-test, 1-tailed	t_{19} = 2.382	P = 0.0139
S3d	Nestin+ NSCs	NTG, PSAPP	Student t-test, 1-tailed	t_{18} = 1.642	P = 0.0590
S3e	Nestin+ NSCs	NTG, PSAPP	Student t-test, 1-tailed	t_{21} = 2.221	P = 0.0187
S3f	Nestin+ NSCs	NTG, Tg2576	Student t-test, 1-tailed	t_{18} = 8.863	P < 0.0001
S4c	Prox1+ hilar granule cells	NTG, APP	Student t-test, 2-tailed	t_{15} = 3.181	P = 0.0062
S5a	Nestin+ BrdU+ NSCs	NTG, APP	Student t-test, 2-tailed	t_{17} = 2.353	P = 0.0309
	BrdU+ Nestin+ NSCs/ Nestin+ NSCs	NTG, APP	Student t-test, 2-tailed	t_{17} = 4.250	P = 0.0005
S5b	Nestin+ BrdU+ NSCs	NTG, APP	Student t-test, 2-tailed	t_{14} = 0.3248	P = 0.7501
	BrdU+ Nestin+ NSCs/ Nestin+ NSCs	NTG, APP	Student t-test, 2-tailed	t_{14} = 2.925	P = 0.0111
S5c	Nestin+ BrdU+ NSCs	NTG, APP	Student t-test, 2-tailed	t_{14} = 2.647	P = 0.0191
	BrdU+ Nestin+ NSCs/ Nestin+ NSCs	NTG, APP	Student t-test, 2-tailed	t_{14} = 1.766	P = 0.0991
S5d	Nestin+ BrdU+ NSCs	NTG, APP	Student t-test, 2-tailed	t_{13} = 2.649	P = 0.0201
	BrdU+ Nestin+ NSCs/ Nestin+ NSCs	NTG, APP	Student t-test, 2-tailed	t_{13} = 0.8650	P = 0.4027
S5e	Nestin+ BrdU+ NSCs	NTG, APP	Student t-test, 2-tailed	t_{21} = 0.8050	P = 0.4299
	BrdU+ Nestin+ NSCs/ Nestin+ NSCs	NTG, APP	Student t-test, 2-tailed	t_{21} = 3.049	P = 0.0061
S6b	BrdU+ Nestin+ NSCs/ Nestin+ NSCs	NTG, APP (saline) NTG, APP (KA)	Kruskal-Wallis test	KW statistic = 26.70	P < 0.0001

		NTG saline v KA APP saline v KA	Dunn post-hoc	Z = 2.795 Z = 2.391	P = 0.0104 P = 0.0336
S6c	BrdU+ Nestin+ ANPs/ Nestin+ ANPs	NTG, APP (saline) NTG, APP (KA)	Kruskal-Wallis test	KW statistic = 27.86	P < 0.0001
		NTG saline v KA APP saline v KA	Dunn post-hoc	Z = 2.651 Z = 2.375	P = 0.0161 P = 0.0351
S7a	ΔFosB IR	NTG, APP (saline) NTG, APP (LEV)	2-way ANOVA	Genotype, $F_{1,35}$ = 35.61 Treatment, $F_{1,35}$ = 10.49 Interaction, $F_{1,35}$ = 9.472	P < 0.0001 P = 0.0026 P = 0.0040
		NTG sal v APP sal NTG LEV v APP LEV	Tukey post-hoc		P < 0.0001 P = 0.2037
S7b	ΔFosB IR	NTG, APP (saline) NTG, APP (LEV)	2-way ANOVA	Genotype, $F_{1,26}$ = 9.096 Treatment, $F_{1,26}$ = 2.391 Interaction, $F_{1,26}$ = 1.729	P = 0.0057 P = 0.1341 P = 0.2001
		NTG sal v APP sal NTG LEV v APP LEV	Tukey post-hoc		P = 0.0316 P = 0.6005
S7d	Spike per hour	Sal (pre, 3d, 8d, 16d) LEV (pre, 3d, 8d, 16d)	2-way ANOVA	Time, $F_{3,12}$ = 18.51 Treatment, $F_{1,4}$ = 18.58 Interaction, $F_{3,12}$ = 6.774	P < 0.0001 P = 0.0125 P = 0.0063
		Sal (pre) v LEV (pre) Sal (3d) v LEV (3d) Sal (8d) v LEV (8d) Sal (16d) v LEV (16d)	Holm-Sidak post-hoc	t_{16} = 0.000 t_{16} = 2.744 t_{16} = 5.377 t_{16} = 3.456	P > 0.9999 P = 0.0286 P = 0.0002 P = 0.0097
S8b	BrdU+ cells	NTG, APP	Student t-test, 2-tailed	t_4 = 0.5571	P = 0.6072
S8c	BrdU+ cells	NTG, APP	Student t-test, 2-tailed	t_6 = 0.7937	P = 0.4576
S9a	Discrimination index	NTG (P1, P2, P3, P4) APP (P1, P2, P3, P4)	2-way ANOVA	Genotype, $F_{1,49}$ = 1.496 Position, $F_{3,49}$ = 9.605 Interaction, $F_{3,49}$ = 0.8249	P = 0.2272 P < 0.0001 P = 0.4865
		NTG v APP (P1) NTG v APP (P2) NTG v APP (P3) NTG v APP (P4)	Fisher's LSD post-hoc	t_{49} = 1.008 t_{49} = 1.757 t_{49} = 0.2310 t_{49} = 0.01285	P = 0.3184 P = 0.0851 P = 0.8183 P = 0.9898
S9b	Time spent with DO	NTG, APP	2-way ANOVA	Genotype, $F_{1,13}$ = 3.357 Test phase, $F_{1,13}$ = 5.206 Interaction, $F_{1,13}$ = 2.399	P = 0.0899 P = 0.0400 P = 0.1454
		NTG v APP (train) NTG v APP (test)	Holm-Sidak post-hoc	t_{26} = 0.1697 t_{26} = 2.388	P = 0.8665 P = 0.0484
S9c	Discrimination index	NTG, APP (saline) NTG, APP (LEV)	2-way ANOVA	Genotype, $F_{1,26}$ = 0.6029 Treatment, $F_{1,26}$ = 5.350 Interaction, $F_{1,26}$ = 20.83	P = 0.4445 P = 0.0289 P = 0.0001
		NTG sal v NTG LEV NTG sal v APP sal NTG sal v APP LEV NTG LEV v APP sal NTG LEV v APP LEV APP sal v APP LEV	Newman-Keuls post-hoc		ns P < 0.01 ns P < 0.05 P < 0.05 P < 0.001
S9d	Time spent with DO	NTG, APP (saline) NTG, APP (LEV)	2-way RM ANOVA	Treatment, $F_{3,26}$ = 8.161 Test phase, $F_{1,26}$ = 59.59 Interaction, $F_{3,26}$ = 8.261	P = 0.0005 P < 0.0001 P = 0.0005
		NTG sal v NTG LEV (train) NTG sal v APP sal (train) NTG sal v APP LEV (train) NTG LEV v APP sal (train) NTG LEV v APP LEV (train) APP sal v APP LEV (train) NTG sal v NTG LEV (test) NTG sal v APP sal (test) NTG sal v APP LEV (test) NTG LEV v APP sal (test) NTG LEV v APP LEV (test) APP sal v APP LEV (test)	Newman-Keuls post-hoc		P > 0.9999 P > 0.9999 P > 0.9999 P > 0.9999 P > 0.9999 P > 0.9999 P = 0.0600 P < 0.0001 P = 0.1300 P = 0.0082 P = 00017 P < 0.0001